Combustion and Flame 158 (2011) 1372–1390

Contents lists available at ScienceDirect

Combustion and Flame

journal homepage: www.elsevier.com/locate/combustflame

Comparison of 2D and 3D density-weighted displacement speed statistics and implications for laser based measurements of flame displacement speed using direct numerical simulation data

N. Chakraborty [a,*], G. Hartung [b], M. Katragadda [a], C.F. Kaminski [b,c]

[a] University of Liverpool, Engineering Department, Brownlow Hill, L69 3GH, UK
[b] University of Cambridge, Department of Chemical Engineering, Pembroke Street, Cambridge CB2 3RA, UK
[c] SAOT School of Advanced Optical Technologies, Friedrich Alexander University Erlangen Nuremberg, 91058 Erlangen, Germany

ARTICLE INFO

Article history:
Received 21 April 2010
Received in revised form 25 September 2010
Accepted 26 November 2010
Available online 30 December 2010

Keywords:
Turbulent premixed flame
Density-weighted displacement speed
Curvature
Direct numerical simulations

ABSTRACT

In a recent study, a light sheet imaging approach has been proposed (Hartung et al., J. Appl. Phys. B 96 (2009) 843–862) which permits measurement of a quantity S_d^{*2D}, which is the two-dimensional projection of the actual density-weighted displacement speed S_d^* for turbulent premixed flames. Here the statistics of S_d^* and S_d^{*2D} are compared using a direct numerical simulation database of statistically planar turbulent premixed flames. It is found that the probability density functions (pdfs) of S_d^{*2D} approximate the pdfs of S_d^* satisfactorily for small values of root-mean-square turbulent velocity fluctuation u', though the S_d^{*2D} pdfs are wider than the S_d^* pdfs. Although the agreement between the pdfs and the standard-deviations of S_d^{*2D} and S_d^* deteriorate with increasing u', the mean values of S_d^{*2D} correspond closely with the mean values of S_d^* for all cases considered here. The pdfs of two-dimensional curvature κ_m^{2D} and the two-dimensional tangential-diffusion component of density-weighted displacement speed S_t^{*2D} are found to be narrower than their three-dimensional counterparts (i.e. κ_m and S_t^* respectively). It has been found that the pdfs, mean and standard-deviation of $\pi/2 \times \kappa_m^{2D}$ and $\pi/2 \times S_t^{*2D}$ faithfully capture the pdfs, mean and standard-deviation of the corresponding three-dimensional counterparts, κ_m and S_t^* respectively. The combination of wider S_d^{*2D} pdfs in comparison to S_d^* pdfs, and narrower S_t^{*2D} pdfs in comparison to S_t^* pdfs, leads to wider $(S_r^* + S_n^*)^{2D} = S_d^{*2D} - S_t^{*2D}$ pdfs than the pdfs of combined reaction and normal-diffusion components of density-weighted displacement speed $(S_r^* + S_n^*)$. This is reflected in the higher value of standard-deviation of $(S_r^* + S_n^*)^{2D}$, than that of its three-dimensional counterpart $(S_r^* + S_n^*)$. However, the mean values of $(S_r^* + S_n^*)^{2D}$ remain close to the mean values of $(S_r^* + S_n^*)$. The loss of perfect correlation between two and three-dimensional quantities leads to important qualitative differences between the $(S_r^* + S_n^*)^{2D} - \kappa_m^{2D}$ and $(S_r^* + S_n^*) - \kappa_m$, and between the $S_d^{*2D} - \kappa_m^{2D}$ and $S_d^* - \kappa_m$ correlations. For unity Lewis number flames, the $S_d^* - \kappa_m$ correlation remains strongly negative, whereas a weak correlation is observed between S_d^{*2D} and κ_m^{2D}. The study demonstrates the strengths and limitations of the predictive capabilities of the planar imaging techniques in the context of the measurement of density-weighted displacement speed, which are important for detailed model development or validation based on experimental data.

1. Introduction

The displacement speed S_d is a quantity of key importance in turbulent premixed combustion [1], which represents the speed with which the flame front moves normal to itself with respect to an initially coincident material surface. Although S_d is a quantity on which turbulent combustion models based on level-set [1] and flame surface density (FSD) methodologies [2,3] critically depend, experimental data on the statistical behaviour of S_d in turbulent flames are rarely presented in the literature [4,5]. For turbulent premixed flames S_d is an inherently three-dimensional quantity and its determination requires the resolution of local flow velocity fields and complete knowledge of the evolving flame geometry. This requires a time-resolved measurement of the three-dimensional flame topology, as well as the full convective flow field. Despite all advances in laser imaging technology for turbulent combustion, attempts to measure three-dimensional displacement speed S_d remain futile. Even if the future brings about the theoretical possibility of measuring S_d, the associated uncertainties

* Corresponding author. Fax: +44 1517944848.
E-mail addresses: n.chakraborty@liverpool.ac.uk (N. Chakraborty), georg.hartung@gmail.com (G. Hartung), m.katragadda@liverpool.ac.uk (M. Katragadda), cfk23@cam.ac.uk (C.F. Kaminski).

0010-2180/$ - see front matter © 2010 The Combustion Institute. Published by Elsevier Inc. All rights reserved.
doi:10.1016/j.combustflame.2010.11.014

Nomenclature

Arabic

C_P	specific heat at constant pressure
C_V	specific heat at constant volume
c	reaction progress variable
c^*	progress variable value defining flame surface
D	progress variable diffusivity
D_0	progress variable diffusivity in the unburned gas
Da	Damköhler number
$h_{\max}$	greater of principal curvatures by magnitude
$h_{\min}$	smaller of principal curvatures by magnitude
k_{global}	global turbulent kinetic energy evaluated over the whole domain
$k_{global,0}$	global turbulent kinetic energy evaluated over the whole domain at initial time
Ka	Karlovitz number
Le	Lewis number
l	integral length scale
$\vec{M}a$	mach number
$\vec{N}$	actual flame normal vector in three-dimensions
$\vec{N}^{2D}$	apparent flame normal vector in two-dimensions
N_i	ith component of flame normal
Pr	Prandtl number
Re_t	turbulent Reynolds number
Sc	Schmidt number
S_d	actual displacement speed in three-dimensions
S_d^*	actual density-weighted displacement speed in three-dimensions
S_d^{2D}	apparent displacement speed in two-dimensions
S_d^{*2D}	apparent density-weighted displacement speed in two-dimensions
S_L	unstrained laminar burning velocity
S_n^*	actual normal diffusion component of density-weighted displacement speed in three-dimensions
S_t^*	actual tangential-diffusion component of density-weighted displacement speed in three-dimensions
S_t^{*2D}	apparent tangential-diffusion component of density-weighted displacement speed in two-dimensions
S_r^*	actual reaction component of density-weighted displacement speed in three-dimensions
$(S_r^*+S_n^*)^{2D}$	apparent combined reaction and normal diffusion component of density- weighted displacement speed in two-dimensions
s_h	shape factor
t_{sim}	simulation time
$\hat{T}$	dimensional temperature
T_{ac}	activation temperature
T_{ad}	adiabatic flame temperature
T_0	reactant temperature
u_i	ith component of fluid velocity
u'	root–mean–square turbulent velocity fluctuation
v_η	Kolmogorov velocity scale
$\dot{w}$	chemical reaction rate of reaction progress variable
x_i	ith Cartesian co-ordinate

Greek

α	angle determining local flame normal orientation
β	angle between $\vec{N}^{2D}$ and $\vec{M}$
β_Z	Zel'dovich number
γ	ratio of specific heats (=C_P/C_V)
δ_{th}	thermal laminar flame thickness
η	Kolmogorov length scale
κ_m	actual flame curvature in three-dimensions
κ_m^{2D}	apparent flame curvature in two-dimensions
κ_1, κ_2	principal curvatures
λ	thermal conductivity
μ	dynamic viscosity
μ_{SD}	mean value of S_d^*/S_L
μ_{SD}^{2D}	mean value of S_d^{*2D}/S_L
μ_{SRN}	mean value of $(S_r^*+S_n^*)/S_L$
μ_{SRN}^{2D}	mean value of $(S_r^*+S_n^*)^{2D}/S_L$
ρ	density
ρ_F	density at the flame front
ρ_0	unburned gas density
σ_{SD}	standard-deviation of S_d^*/S_L
σ_{SD}^{2D}	standard-deviation of S_d^{*2D}/S_L
σ_{SRN}	standard-deviation of $(S_r^*+S_n^*)/S_L$
σ_{SRN}^{2D}	standard-deviations of $(S_r^*+S_n^*)^{2D}/S_L$
Σ	flame surface density based on fine-grained description
Σ_{gen}	generalised flame surface density
τ	heat release parameter

Acronyms

DNS	direct numerical simulation
PLIF	planar laser induced fluorescence
2D	two-dimensional/two-dimensions
3D	three-dimensional/three dimensions

will, in all likelihood, limit the usefulness of the measurements. In a recent paper, Hartung et al. [5] presented an alternative methodology of measuring a quantity related to the density-weighted displacement speed $S_d^* = \rho_F S_d/\rho_0$ based on previously developed techniques for the time-resolved planar imaging of the flame front contour [6–12] via laser induced fluorescence (LIF) of OH and simultaneously performed stereoscopic Particle Image Velocimetry (PIV). This yields a quantity S_d^{*2D} which can be thought of as a projection of S_d^* onto the plane defined by the laser sheet. The quantity S_d^{*2D} can be interpreted as a two-dimensional, density-weighted displacement speed, which can potentially be used for calibrating and validating turbulent combustion models. It was indicated in Ref. [5] that for flames with symmetry (e.g. jet flames with statistical symmetry around the jet axis) the statistics of S_d^{*2D} may represent the true statistics of S_d^* under certain conditions. As S_d^{*2D} can be extracted from experimental data with relative ease and high accuracy, it is important to assess the differences between S_d^{*2D} and its actual three-dimensional counterpart. This is not only of the interest to experimentalists but also for the modelling community because the present study demonstrates the extent to which the statistics of two-dimensional displacement speed S_d^{*2D} faithfully mimic the statistics of the actual three-dimensional density-weighted displacement speed S_d^*. However, a quantitative analysis of the differences between the statistical behaviours of S_d^* and S_d^{*2D} is not possible by experimental means alone and this motivated the current study, where direct numerical simulation (DNS) data has been used to explore the relation between S_d^* and S_d^{*2D} directly.

To achieve this goal, S_d^* and S_d^{*2D} data were extracted from a DNS database of statistically planar freely propagating turbulent premixed flames. The data is analysed in terms of the probability density functions (pdfs) of density-weighted values of the actual displacement speed (i.e. S_d^*) and its two-dimensional projection (i.e. S_d^{*2D}). Differences between the pdfs of S_d^* and S_d^{*2D} are analysed in detail and the physical origins for the observed differences are identified. Moreover, the pdfs of the actual and two-dimensional projections of reaction, normal-diffusion and tangential-diffusion components of density-weighted displacement speed are analysed in detail. A simple correction is then proposed which permits the extraction of the actual density-weighted tangential-diffusion component of displacement speed S_t^* and flame curvature κ_m pdfs from their two-dimensional counterparts. These results offer information about the validity and importance of S_d^{*2D} as a parameter, which can potentially provide qualitatively similar information as S_d^*, while being experimentally accessible with currently available technology and good measurement precision. However, the present results also show that some three-dimensional information is necessarily lost in two-dimensional measurements of S_d^{*2D}. As a result, the statistics of the combined reaction and normal-diffusion components $(S_r^* + S_n^*)$ cannot be recovered in a straightforward manner from their two-dimensional counterparts. Moreover, it has been demonstrated that the correlation between the two-dimensional curvature κ_m^{2D} and S_d^{*2D} do not capture the actual curvature κ_m dependence of S_d^* and physical explanations are provided for the observed differences.

2. Mathematical background

In premixed combustion, the species field is often normalised to define a reaction progress variable c using a suitable reactant mass fraction Y_R in the following manner: $c = (Y_{R0} - Y_R)/(Y_{R0} - Y_{R\infty})$ where subscripts 0 and ∞ are used to denote values in unburned gases and fully burned products respectively. The transport equation of c is given by:

$$\rho[\partial c/\partial t + u_j \partial c/\partial x_j] = \dot{w} + \partial[\rho D \partial c/\partial x_j]/\partial x_j, \tag{1}$$

which can be rewritten in kinematic form for a given $c = c^*$ isosurface as:

$$\partial c/\partial t + u_j \partial c/\partial x_j|_{c=c^*} = S_d|\nabla c||_{c=c^*} \quad \text{where} \quad S_d = (\dot{w} + \nabla.(\rho D \nabla c))/\rho|\nabla c||_{c=c^*} \tag{2i}$$

If the $c = c^*$ isosurface is considered to be the flame surface, the density-weighted displacement speed is given by: $S_d^* = \rho_F S_d/\rho_0$ [5,13–21], where ρ_F and ρ_0 are the densities at the flame surface and in the unburned gas, respectively. The density-weighted displacement speed is often used in level-set [1,22] and FSD [2,3,23–29] based modelling approaches.

The statistical behaviour of the surface density function (SDF $= |\nabla c|$) [30] transport is significantly affected by strain rate and curvature dependencies of displacement speed. This was demonstrated in Refs. [23,24,27,28] by analysing the statistics of the various terms of the SDF transport equation:

$$\frac{\partial}{\partial t}|\nabla c| + \frac{\partial}{\partial x_j}(u_j|\nabla c|) = (\delta_{ij} - N_i N_j)\frac{\partial u_i}{\partial x_j}|\nabla c| + S_d \frac{\partial N_i}{\partial x_i}|\nabla c| - \frac{\partial}{\partial x_i}(S_d N_i |\nabla c|) \tag{2ii}$$

where $\vec{N} = -\nabla c/|\nabla c||_{c=c^*}$ is the local flame normal. Eq. (2ii) has also been obtained while deriving the transport equation of the FSD based on its fine-grained description $\Sigma = \overline{|\nabla c|\delta(c - c^*)}$ in previous studies [31–33]. In Eq. (2ii), the first term on the left-hand side is the transient term and the second represents the advection term. The first term on the right-hand side relates to the generation of scalar gradients due to straining, the second term to the generation or destruction of scalar gradients due to curvature stretch and the third term relates to propagation. Based on the definition of the displacement speed, the mean reaction rate in turbulent premixed flames can be written as

$$\overline{\dot{w}} + \overline{\nabla.(\rho D \nabla c)} = \overline{(\rho S_d)}_s \Sigma_{gen} \tag{2iii}$$

where Σ_{gen} is the generalised FSD which is given by [34]:

$$\Sigma_{gen} = \overline{|\nabla c|} \tag{2iv}$$

The overbars in Eqs. (2iii) and (2iv) indicate either a Reynolds averaging or LES filtering operation as appropriate. The quantity $\overline{(Q)}_s = \overline{Q|\nabla c|}/\Sigma_{gen}$ represents the surface averaged value of a general quantity Q [34,35]. Eq. (2iii) suggests that the mean reaction rate $\overline{\dot{w}}$ can be closed with the help of the generalised FSD if both the generalised FSD and the surface averaged value of density-weighted displacement speed ρS_d (i.e. $\overline{(\rho S_d)}_s$) are adequately modelled. Under some conditions it may be necessary to solve a transport equation for the generalised FSD, which takes the following form upon Reynolds averaging/LES filtering of Eq. (2ii) [2,3]:

$$\frac{\partial \Sigma_{gen}}{\partial t} + \frac{\partial}{\partial x_i}(\tilde{u}_i \Sigma_{gen}) + \frac{\partial}{\partial x_i}\left(\left(\overline{(u_i)}_s - \tilde{u}_i\right)\Sigma_{gen}\right) = \overline{\left((\delta_{ij} - N_i N_j)\frac{\partial u_i}{\partial x_j}\right)}_s \Sigma_{gen} - \frac{\partial}{\partial x_i}(\overline{(S_d N_i)}_s \Sigma_{gen}) + \overline{\left(S_d \frac{\partial N_i}{\partial x_i}\right)}_s \Sigma_{gen} \tag{2v}$$

where $\tilde{Q}$ indicates the Favre averaged value of a general quantity given by $\tilde{Q} = \overline{\rho Q}/\bar{\rho}$. The transport equation of FSD based on its fine-grained description (i.e. $\Sigma = \overline{|\nabla c|\delta(c - c^*)}$) [31–33,35] takes the same form as that of Eq. (2v) and can be obtained by replacing Σ_{gen} with Σ. The terms on the left-hand side of Eq. (2v) are the transient term, the resolved convection term and the sub-grid convection term. On the right-hand side, the terms are referred to as the strain rate term, the propagation term and the curvature term, respectively. Eq. (2v) clearly suggests that the statistical behaviour of displacement speed plays a crucial role in the behaviour of the curvature and propagation terms of the FSD transport equation [23–29]. Displacement speed also appears in the governing equation for the level-set (G-equation) approach [1,22]:

$$\frac{\partial G}{\partial t} + u_j \frac{\partial G}{\partial x_j} = S_d|\nabla G| \tag{2vi}$$

From Eqs. (2v) and (2vi), it is evident that displacement speed plays a crucial role in all of the FSD and level-set methods of reaction rate closure. A number of recent studies [23–28] have demonstrated that curvature and strain rate dependence eventually determines the strain rate and curvature dependences of the curvature and propagation terms (i.e. $\overline{\left(S_d \nabla \cdot \vec{N}\right)}_s \Sigma_{gen}$ and $-\nabla \cdot [\overline{(S_d \vec{N})}_s \Sigma_{gen}]$ respectively) of the FSD transport equation. The above discussion clearly demonstrates the need for accurate experimental measurement of displacement speed, which acts as a backbone in both G-equation and FSD based modelling methodologies.

It is evident from Eq. (2i) that the statistical behaviour of S_d (and thus S_d^*) depends on the relative balance between $\dot{w}$ and $\nabla.(\rho D \nabla c)$. Thus it is often useful to decompose S_d^* into the reaction, normal-diffusion and tangential-diffusion components (i.e. S_r^*, S_n^* and S_t^* respectively) as [14–29]:

$$S_d^* = S_r^* + S_n^* + S_t^*, \tag{3}$$

where

$$S_r^* = \dot{w}/\rho_0|\nabla c||_{c=c^*}; S_n^* = \vec{N}.\nabla(\rho D \vec{N}.\nabla c)/\rho_0|\nabla c||_{c=c^*} \quad \text{and} \quad S_t^* = -2\rho D \kappa_m/\rho_0, \tag{4}$$

with $\kappa_m = 0.5 \times \nabla.\vec{N}|_{c=c^*} = 0.5 \times (\kappa_1 + \kappa_2)$ representing the arithmetic mean of two principal curvatures κ_1 and κ_2. The quantity κ_m will henceforth be referred to as curvature in this paper.

The decomposition of S_d^* into the reaction, normal-diffusion and tangential-diffusion components (i.e. S_r^*, S_n^* and S_t^* respectively) [13–19], as shown in Eq. (4), is important from the point of view of level-set (G-equation) modelling [1,22] which was discussed in detail by Peters [1]. Several studies [2,3,21,23–29] have demonstrated the usefulness of such a decomposition for the modelling of the curvature and propagation terms of the FSD transport equation. Thus it is useful and timely to examine whether accurate statistical information on various components of displacement speed can be obtained from their two-dimensional counterparts. This will be addressed in greater detail in Sections 3 and 5 of this paper.

3. Relation with measureable quantities

For a full review of the experimental approach the reader is referred to Ref. [5]. A representative three-dimensional view of the flame surface, measurement plane, relevant co-ordinates and angles are shown in Fig. 1a and b. In three-dimensions the flame moves with the propagation velocity $\vec{u} + S_d \vec{N}$. The displacement velocity of the flame with respect to an initially coincident material surface can be written as $S_d \vec{N}$ [31,32]. In Ref. [5], the flame propagation and the local velocity measurements have been carried out simultaneously for a given c isosurface (i.e. OH reaction layer indicating the c isosurface close to maximum heat release). Subsequently the projection of the local fluid velocity onto the measurement plane is subtracted from the flame propagation velocity in two-dimensions in order to obtain the two-dimensional displacement speed S_d^{*2D}. The two-dimensional measurement plane defined by the light sheet is taken to be the $x_1 - x_2$ plane in Fig. 1a and b. With reference to Fig. 1a if the point A on the flame surface moves along the local flame normal direction in quiescent flow (i.e. $\vec{u} = 0$), the distance AB by which flame moves in time Δt will be given by $S_d \Delta t$. During a light sheet measurement this movement will be observed to cover the distance AC in the measurement plane. According to Fig. 1a, the local flame vector $\vec{N}$ at point A is directed along the direction given by AB whereas the apparent flame normal vector in two-dimensions $\vec{N}^{2D}$ is directed along the direction given by AC. Using the right angled triangle ABC and standard trigonometric relations the distance AC is found to be $S_d \Delta t / \cos\alpha$. Hence the apparent displacement speed in two-dimensions is

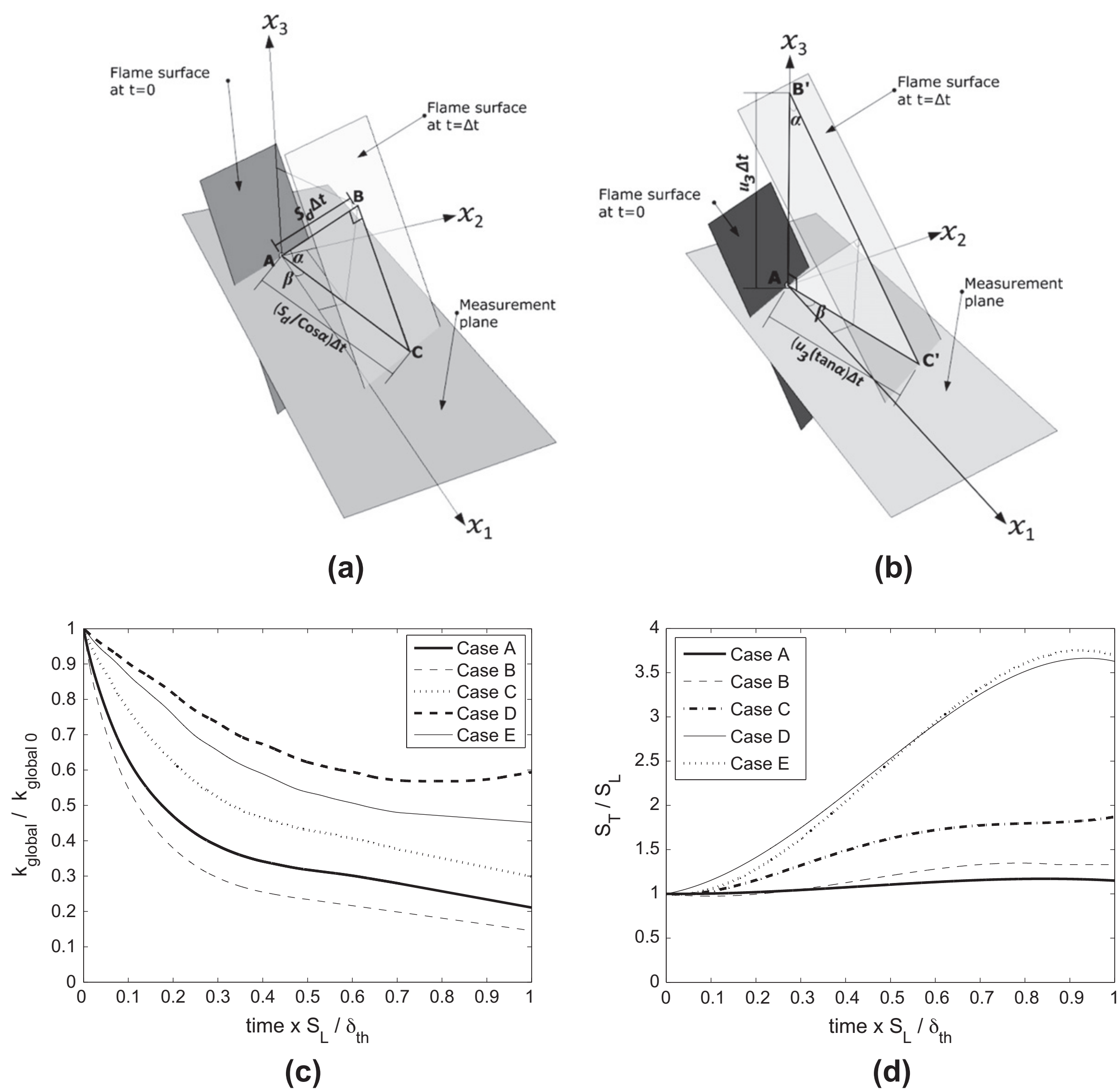

Fig. 1. (a and b) Schematic diagrams which explain Eq. (5). The two-dimensional measurement plane is defined by the light sheet (e.g. the $x_1 - x_2$ plane in this case). The x_3 direction is perpendicular to the measurement plane. (a) Effect of flame normal movement on the expression of the two-dimensional projection of displacement speed S_d^{2D}. According to Fig. 1a, the local flame vector $\vec{N}$ at point A is directed along the direction given by AB whereas the apparent flame normal vector in two-dimensions $\vec{N}^{2D}$ is directed along the direction given by AC. The angle α is the angle between AB and AC. The angle β is the angle between AC and x_1-direction which is taken to coincide with the mean direction of flame propagation; (b) Effect of out-of-plane convection on the expression of the two-dimensional projection of displacement speed S_d^{2D} due to the velocity component u_3. According to Fig. 1b, the apparent flame normal vector in two-dimensions $\vec{N}^{2D}$ is directed along the direction given by AC′. Temporal evolutions of (c) global turbulent kinetic energy evaluated over the whole domain normalised by its initial value $k_{global}/k_{global,0}$ and (d) normalised turbulent flame speed S_T/S_L.

given as: $AC/\Delta t = S_d/\cos\alpha$. Figure 1b shows the situation in the case of out-of-plane convection. Due to out-of-plane convection if the point A moves a distance AB′ in a time interval Δt then even in the absence of flame normal propagation, the movement along the apparent two-dimensional normal direction (i.e. $\vec{N}^{2D}$ direction) is $AC' = (u_3 \tan\alpha)\Delta t$ (using the right angled triangle AB′C′). Thus the apparent two-dimensional displacement speed will be $AC'/\Delta t = (u_3 \tan\alpha)$. Combining the situations depicted in Fig. 1a and b an apparent two-dimensional displacement speed S_d^{2D} can be defined in the following manner [5]:

$$S_d^{2D} = (S_d/\cos\alpha) + u_3 \tan\alpha \tag{5}$$

The flame normal components according to Fig. 1a and b are given by:

$$N_1 = \cos\alpha\cos\beta; \quad N_2 = \cos\alpha.\sin\beta \text{ and } N_3 = \sin\alpha \tag{6}$$

where $|\beta|$ is given by $\cos^{-1}|\vec{N}^{2D}.\vec{M}|$ where $\vec{N}^{2D}$ is the apparent flame normal vector in the two-dimensional projection and $\vec{M}$ is the unit vector in the direction of mean flame propagation, which is taken to be the x_1-direction for the statistically planar turbulent premixed flames considered here. A similar formula for the two-dimensional projection of displacement speed (i.e. $S_d^{2D} = S_d/\cos\alpha$) was recently used by Hawkes et al. [36] which neglected the effects of out-of-plane convection. It is worth noting from Eqs. (5) and (6) that a singularity in the expression of S_d^{2D} may arise when cos α approaches to zero (i.e. $\cos\alpha \to 0$) and thus care needs to be taken to choose a measurement plane for the flame under study to avoid this possibility. Problems are minimised if the direction of mean flame propagation (here the x_1-direction) is known for the experimental set up. A two-dimensional projection on the plane containing the mean flame propagation direction should then be used for the measurement S_d^{2D}. This aspect will be addressed again in Section 5 of this paper.

Following on from above the density-weighted two-dimensional displacement speed S_d^{*2D} can be written as: $S_d^{*2D} = \rho_F S_d^{2D}/\rho_0$. A two-dimensional curvature can be defined, based on the apparent flame normal vector $\vec{N}_{2D}$, as: $\kappa_m^{2D} = 0.5 \times \nabla\cdot\vec{N}_{2D}$. This can then be used to obtain an apparent two-dimensional density-weighted tangential-diffusion component of displacement speed:

$$S_t^{*2D} = -2\rho D\kappa_m^{2D}/\rho_0 \tag{7}$$

Thus the apparent two-dimensional combined reaction and normal-diffusion components of density-weighted displacement speed can be extracted as:

$$(S_r^* + S_n^*)^{2D} = S_d^{*2D} - S_t^{*2D} = S_d^{*2D} + 2\rho D\kappa_m^{2D}/\rho_0 \tag{8}$$

The statistics of S_d^{*2D}, S_t^{*2D} and $(S_r^* + S_n^*)^{2D}$ will be explored in detail in Section 5 of this paper along with their relations to actual S_d^*, S_t^* and $(S_r^* + S_n^*)$ respectively. It is important to note that all quantities defined by Eqs. (6)–(8) can be determined robustly from experimental measurements using the approach outlined in Ref. [5].

4. Numerical implementation

A DNS database of freely-propagating statistically planar turbulent premixed flames under decaying turbulence has been considered for this study. Simulations were carried out using a three-dimensional compressible DNS code called SENGA [2,3,19–21,23–25,27,28]. The standard conservation equations of mass, momentum energy and species for compressible reacting flows are solved in non-dimensional form. In SENGA [2,3,19–21,23–25,27,28] all the velocity scales are normalised with respect to unstrained laminar burning velocity S_L. The pre-exponential factor for the Arrhenius type chemical reaction is modulated to result in the desired unstrained laminar burning velocity S_L for the given value of thermal diffusivity. The spatial discretisation is carried out using a 10th central difference scheme for the internal grid points and the order of the numerical differentiation gradually decreases to a one sided 2nd order scheme to non-periodic boundaries. The time advancement is taken care of in an explicit manner using a 3rd order low storage Runge–Kutta scheme [37]. The turbulent velocity field is initialised using a standard pseudo-spectral method [38] following Batchelor–Townsend spectrum [39], whereas the flame is initialised by a steady unstrained laminar flame solution. The simulation domain is taken to be a rectangular parallelepiped with size $36.2\delta_{th} \times 24.1\delta_{th} \times 24.1\delta_{th}$ which is discretised by a Cartesian grid of size $345 \times 230 \times 230$ with uniform grid spacing in each direction where $\delta_{th} = (T_{ad} - T_0)/Max|\nabla\hat{T}|_L$ is the thermal flame thickness and T_0, T_{ad} and $\hat{T}$ are the unburned gas, adiabatic flame, and the instantaneous temperatures, respectively. The boundaries in the direction of mean flame propagation (i.e. x_1-direction) are taken to be partially-non-reflecting whereas the transverse directions (i.e. x_2 and x_3 directions) are considered to be periodic. Standard Navier–Stokes Characteristic Boundary-Conditions [40] have been used for specifying partially non-reflecting boundaries. In this study the chemical mechanism is simplified by a single-step Arrhenius type reaction for computational economy as done in several previous studies [2,3,19–21,23–25,27–29,35,41]. For the present thermo-chemistry the maximum reaction rate is attained close to $c = 0.8$ [19–21,23–25,27–29] and thus the $c = 0.8$ isosurface will henceforth be taken as the flame surface in this paper. The grid spacing is determined by the resolution of the flame and about 10 grid points are kept within δ_{th} for all cases. The initial values for the rms turbulent velocity fluctuation normalised by unstrained laminar burning velocity u'/S_L and the integral length scale to flame thickness ratio l/δ_{th} are presented in Table 1 along with the values of Damköhler number $Da = l\cdot S_L/u'\delta_{th}$, Karlovitz number $Ka = (u'/S_L)^{3/2}(l/\delta_{th})^{-1/2}$ and turbulent Reynolds number $Re_t = \rho_0 u' l/\mu_0$. The simulation parameters are chosen in such a manner that a variation of turbulent Reynolds number Re_t from 20 to 100 was obtained by independently changing Damköhler and Karlovitz numbers. Standard values are taken for Prandtl number Pr, ratio of specific heats $\gamma = C_P/C_V$ and the Zel'dovich number $\beta_Z = T_{ac}(T_{ad} - T_0)/T_{ad}^2$ (i.e. $Pr = 0.7$, $\gamma = 1.4$, $\beta_Z = 6.0$). The Lewis number Le is taken to be unity for all the species. From Table 1, it is evident that Ka remains greater than unity for all cases, which indicates that the combustion situation belongs to thin reaction zones on the regime diagram by Peters [1]. In all cases flame–turbulence interactions take place under conditions of decaying turbulence for which, simulations should be carried out for a duration $t_m = Max(t_f, t_f)$, where $t_f = l/u'$ is the initial eddy turn over time and $t_c = \delta_{th}/S_L$ is the chemical time scale. For all cases, the simulation time is equivalent to one chemical time scale, i.e. $t_{sim} = t_c$. This corresponds to $2.0t_f$ for case D, $3.0t_f$ for cases A, C, E and $4.34t_f$ for case B. Although the simulation varies when measured in terms of the number of eddy turn over times for the different cases, the thermo-chemistry remains same for all flames, and the time $t = \delta_{th}/S_L$ corresponds to same duration of flame–turbulence interaction for all cases. It is worth noting that for the present thermo-chemistry the thermal flame thickness δ_{th} is given by: $\delta_{th} = 1.785D_0/S_L$. Thus the present simulation time $t_{sim} = t_c$

Table 1
Initial simulation parameters and non-dimensional numbers relevant to the present DNS database.

Case	u'/S_L	l/δ_{th}	τ	Re_t	Da	Ka
A	5.0	1.67	4.5	22	0.33	8.67
B	6.25	1.44	4.5	23.5	0.23	13.0
C	7.5	2.5	4.5	49.0	0.33	13.0
D	9.0	4.31	4.5	100.0	0.48	13.0
E	11.25	3.75	4.5	110	0.33	19.5

corresponds to about two Zel'dovich chemical timescales (i.e. $t_{sim} = t_c = \delta_{th}/S_L = 1.785D_0/S_L^2$). The present simulation time in terms of both eddy turn over times and chemical time scale is comparable to the simulation times used in several previous and contemporary DNS studies [13–21,23–29,33,34,41–46]. It is admitted that longer simulation times have been reported for some configurations (e.g. the Bunsen burner flame in Ref. [36]) but such simulations are highly computationally expensive and would prohibit an extensive parametric studies as carried out in the current study, with reasonable computational economy.

Values for u'/S_L, l/δ_{th} and δ_{th}/η when statistics are extracted have been presented in Table 2. It can be seen from Table 2 that for all cases the thermal flame thickness δ_{th} remains greater than the Kolmogorov length scale η when statistics were collected. This suggests that the combustion situation in all cases belongs to the thin reaction zones regime [1] when statistics were extracted. The temporal evolution of turbulent kinetic energy evaluated over the whole domain normalised by its initial value (i.e. $k_{\text{global}}/k_{\text{global0}}$) is shown in Fig. 1c which shows that the global turbulent kinetic energy was not varying rapidly when the statistics were extracted. The temporal variation of the global turbulent kinetic energy was found to be consistent with several previous studies [19,23,47]. It is evident from Table 2 that the value of global turbulent velocity fluctuation level had decayed by 53%, 61%, 45%, 24% and 34% in comparison to their initial values for cases A-E respectively by the time statistics were extracted. By contrast, the integral length scale increased by factors between 1.5–2.25 ensuring sufficient numbers of turbulent eddies were retained in each direction to obtain useful statistics. The temporal evolution of turbulent flame speed normalised by unstrained laminar burning velocity (i.e. S_T/S_L) for all the cases are shown in Fig. 1d where S_T is evaluated as $S_T = (1/\rho_0 A_P)\int_V \dot{w}d\vartheta$, in which A_P is the projected area of the flame in the direction of mean flame propagation. It is evident from Fig. 1d that the turbulent flame speed S_T was no longer changing rapidly with time when statistics were extracted. It will be demonstrated later in Section 5 that the qualitative nature of the statistics presented in this paper remained unchanged since $t = 0.5\delta_{th}/S_L = 0.89D_0/S_L$ for all cases. The time $t = 0.5\delta_{th}/S_L$ is equivalent to $1.0t_f$ in case D, $1.5t_f$ in cases A, C, E and $2.17t_f$ for case B.

It is important to note the length scale separation between the integral length scale l and the Kolmogorov length scale η is limited by the turbulent Reynolds number (e.g. $l/\eta \sim \text{Re}_t^{3/4}$). For non-reacting DNS simulations the grid spacing Δx needs to be smaller than the Kolmogorov length scale η. On the other hand, it is necessary to include a sufficient number of integral-scale eddies within the domain in order to ensure a sufficient number of statistically independent samples. If a total of n_l turbulent eddies are accommodated within the domain then the grid size N in each direction is given by: $N \geqslant n_l l/\eta$ which can be rewritten as $N \geqslant n_l \text{Re}_t^{3/4}$ using the turbulence scaling law $l/\eta \sim \text{Re}_t^{3/4}$. Moreover, in combustion DNS the flame thickness δ_{th} based on the maximum value of the reaction progress variable gradient needs to be resolved using a minimum of 10 grid points so the grid spacing needs to be less than $\delta_{th}/10$, which yields the grid size requirement $N \geqslant n_l 10 l/\delta_{th}$ or alternatively $N \geqslant n_l 10\text{Re}_t^{3/4}/Ka^{1/2}$. This suggests that the grid size requirement for combustion DNS is more demanding than for non-reacting DNS when $Ka < 100$. This suggests that the range of the values of u'/S_L, l/δ_{th}, Re_t used in the present study is determined by computational economy of carrying out three-dimensional DNS simulations. Moreover, in order to carry out an extensive parametric study as done in the current article, a large number of cases need to be run within reasonable computational cost. It is important to note that the turbulent Reynolds number Re_t values used in this study are either comparable to or greater than many previous DNS studies that have contributed significantly to the understanding of turbulent combustion [13–21,23–29,33,34,41–46,48,49]. It is furthermore worth noting that good agreement was obtained between experimental and DNS data in a number of previous studies despite prevailing differences in turbulent Reynolds number Re_t [50–52].

Table 2
Values of u'/S_L, l/δ_{th} and δ_{th}/η when the statistics were extracted (i.e. $t = \delta_{th}/S_L$).

Case	u'/S_L	l/δ_{th}	δ_{th}/η
A	2.37	2.51	3.41
B	2.43	1.68	4.24
C	4.13	2.53	4.50
D	6.83	9.68	4.51
E	7.44	5.17	5.63

5. Results and discussion

5.1. Flame–turbulence interactions

The contours of c at the central $x_1 - x_2$ plane at $t = 1.0\delta_{th}/S_L$ are shown in Fig. 2a–e for cases A–E respectively. Figure 2a–e shows that the wrinkling of c isosurfaces increases with u' and the contours of c representing the preheat-zone (i.e. $c < 0.5$) are much more distorted than those representing the reaction zone (i.e. $0.7 \leqslant c \leqslant 0.9$). This tendency is more prevalent for high Ka flames because δ_{th} remains greater than the Kolmogorov length scale η in the thin reaction zone regime [1]. Under these conditions, energetic turbulent eddies enter the preheat-zone and cause unsteady fluctuations and flame distortion while the reaction zone retains its quasi-laminar structure. The scale separation between δ_{th} and η increases with increasing Ka, allowing more energetic eddies to enter into the flame which in turn causes more severe distortion of the flame for high values of Karlovitz number.

All the statistics in this study will be presented for the $c = 0.8$ isosurface because the maximum reaction rate for the present thermo-chemistry takes place close to $c = 0.8$ [23,25]. This is consistent with the experimental conditions reported in Ref. [5], where time-resolved planar imaging of the flame front contour via OH LIF is used to track the reaction progress variable isosurface corresponding to the maximum reaction rate. Moreover, in the context of the level-set method [1,22] and fine-grained FSD i.e. $\Sigma = \overline{|\nabla c|\delta(c - c^*)}$) based reaction rate closure [35] the most reactive c isosurface is taken to be the flame surface and the density-weighted displacement speed S_d^* for that location is of primary importance [1,22,35]. For these reasons the local statistics of S_d^* for the most reactive isosurface have been presented in a number of previous studies [13–18] and the same approach is followed here. Although the flame speed statistics are presented only for the $c = 0.8$ isosurface, the same qualitative trends have been observed for other c isosurfaces across the flame brush.

PLIF of the OH-radical (OH-PLIF) is commonly employed in premixed combustion diagnostics, because the location of the maximum gradient in OH-concentration can be used as an indicator of the location of the reaction zone or flame front. For the present flame conditions the suitability of OH-PLIF to mark the reaction zone has been extensively validated [50–57] and found optimal, yielding high signal levels and exhibiting only a weak dependence of signals to changes in curvature and strain rate.

5.2. Comparison between S_d^* and S_d^{*2D} pdfs

The pdfs of three-dimensional density-weighted (normalised) displacement speed S_d^*/S_L and two-dimensional projection of density-weighted (normalised) displacement speed S_d^{*2D}/S_L at the $c = 0.8$ isosurface are shown in Fig. 3a–c for cases A, C and E. Pdfs

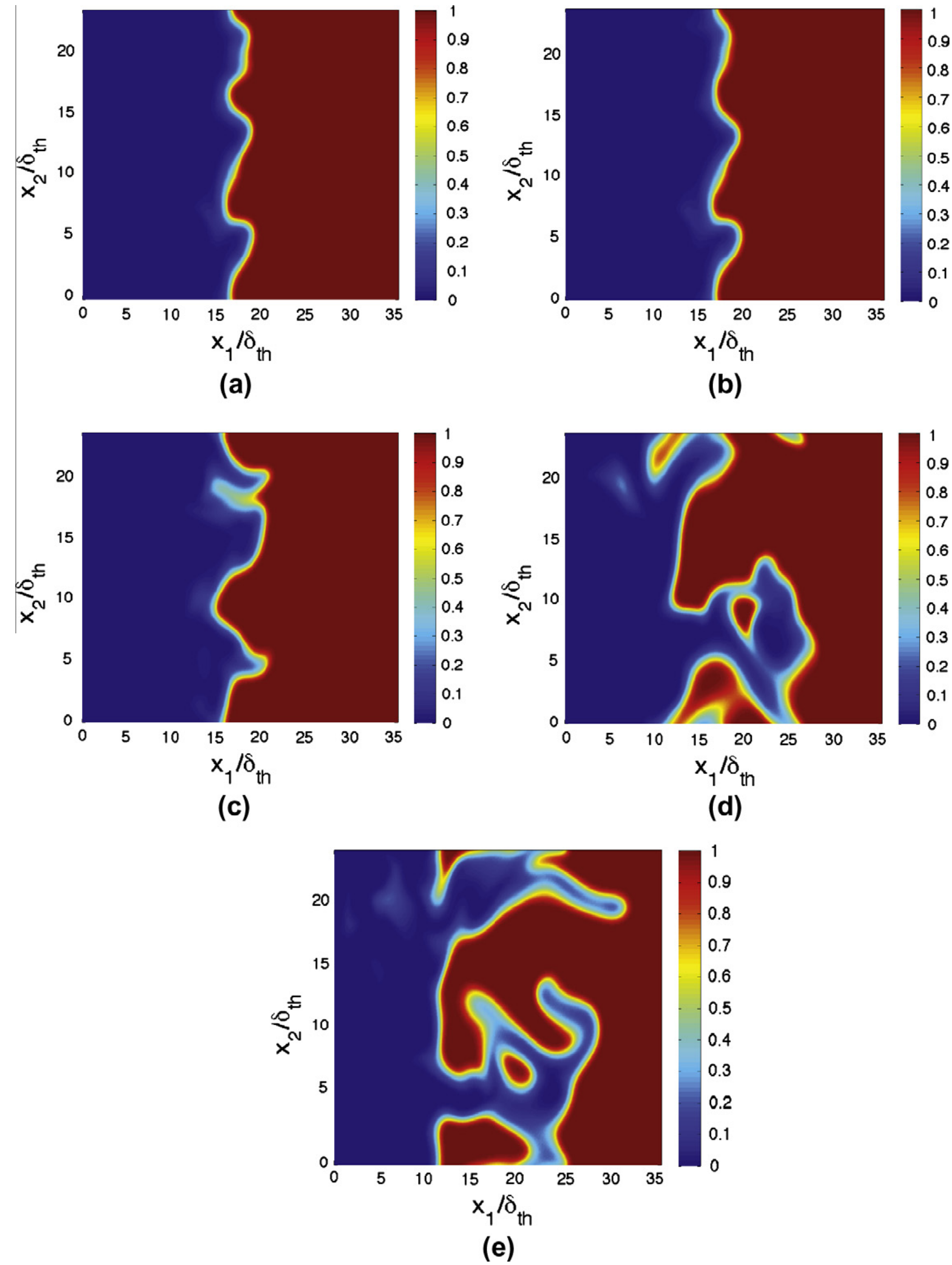

Fig. 2. Contours of c in the central mid-plane of the domain at time $t = \delta_{th}/S_L$ for cases: (a) A; (b) B; (c) C; (d) D; (e) E.

of S_d^{*2D}/S_L are extracted from data collected from two-dimensional planes containing the direction of mean flame propagation (i.e. x_1-direction). Cases B and D are not shown explicitly because they were found to be qualitatively similar to the cases A and E, respectively. In the present study it is assumed that the flame propagation and the local velocity measurements have been carried out simultaneously for a given c isosurface (i.e. OH reaction layer indicating the c isosurface close to maximum heat release) and the local fluid velocity projection in two-dimensions is subtracted from the flame propagation velocity in two-dimensions in order to obtain displacement speed for a given c isosurface in two-dimensional projection as done in Ref. [5]. For the sake of convenience, the terminologies associated with Fig. 1 will be followed in the following discussion where the flame is assumed to be projected on the $x_1 - x_2$ plane whereas the mean direction of flame propagation is assumed to align with the x_1-direction. Figure 3a–c shows that the most probable value of normalised density-weighted displacement speed S_d^*/S_L remains of the order of unity

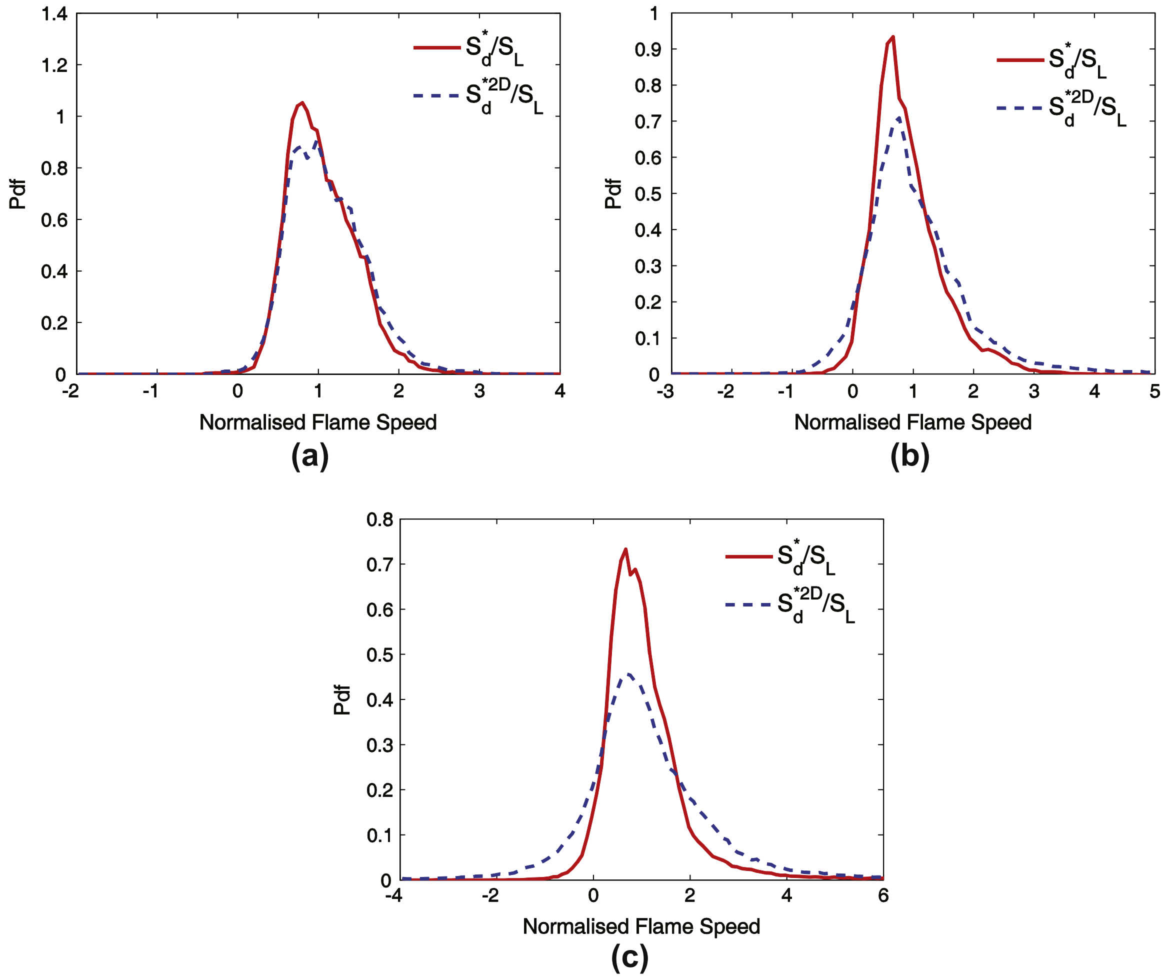

Fig. 3. Pdfs of S_d^*/S_L and S_d^{*2D}/S_L on the $c = 0.8$ isosurface for cases: (a) A; (b) C; (c) E. All the pdfs and joint pdfs of this figure and the subsequent figures are extracted at time $t = \delta_{th}/S_L$.

Table 3
Relevant mean values and standard-deviations of flame speeds on the $c = 0.8$ isosurface when statistics were extracted (i.e. $t_{sim} = \delta_{th}/S_L$).

Case	μ_{SD}	σ_{SD}	μ_{SD}^{2D}/μ_{SD}	$\sigma_{SD}^{2D}/\sigma_{SD}$	$\pi/2 \times \sigma_{ST}^{2D}/\sigma_{ST}$	μ_{SRN}	σ_{SRN}	μ_{SRN}^{2D}/μ_{SRN}	$\sigma_{SRN}^{2D}/\sigma_{SRN}$
A	1.0	0.41	1.06	1.12	1.14	1.0	0.16	1.05	1.94
B	1.0	0.43	1.06	1.13	1.14	1.0	0.19	1.06	2.00
C	0.95	0.61	1.09	1.33	1.29	0.97	0.37	1.10	2.04
D	0.90	0.66	1.07	1.70	1.34	0.90	0.55	1.04	2.07
E	0.97	0.82	1.07	1.50	1.32	0.93	0.62	1.05	2.10

for all cases but the spread of the pdf increases with u'/S_L. The mean and the standard-deviation of normalised density-weighted displacement speed S_d^*/S_L (i.e. μ_{SD} and σ_{SD}) at the time when statistics were extracted (i.e. $t = \delta_{th}/S_L$) for all cases are listed in Table 3, which substantiates that μ_{SD} remains of the order of unity for all cases and σ_{SD} increases with increasing u'. Similar behaviour has been observed for other c isosurfaces across the flame brush (see Table A1 in Appendix A). The values of μ_{SD} and σ_{SD} halfway through the simulation (i.e. $t = 0.5\delta_{th}/S_L$) are shown in Table 4 for the $c = 0.8$ isosurface which shows μ_{SD} assumed values close to but less than unity. Moreover, σ_{SD} did not exhibit any monotonic trend with u'. At $t = 0.5\delta_{th}/S_L$, the flame–turbulence interaction was developing, which attributes to the observed differences in behaviours of μ_{SD} and σ_{SD} between times $t = 0.5\delta_{th}/S_L$ and $t = \delta_{th}/S_L$.

Table 4
Relevant mean values and standard-deviations of flame speeds on the $c = 0.8$ isosurface halfway through the simulation (i.e. $t = 0.5\delta_{th}/S_L$).

Case	μ_{SD}	σ_{SD}	μ_{SD}^{2D}/μ_{SD}	$\sigma_{SD}^{2D}/\sigma_{SD}$	$\pi/2 \times \sigma_{ST}^{2D}/\sigma_{ST}$	μ_{SRN}	σ_{SRN}	μ_{SRN}^{2D}/μ_{SRN}	$\sigma_{SRN}^{2D}/\sigma_{SRN}$
A	0.93	0.52	1.05	1.15	1.12	0.94	0.27	1.05	1.86
B	0.93	0.57	1.05	1.17	1.15	0.93	0.30	1.06	1.88
C	0.86	0.74	1.01	1.36	1.20	0.85	0.48	0.97	2.00
D	0.80	0.55	1.04	2.11	1.22	0.80	0.34	1.03	3.25
E	0.77	0.82	1.06	2.33	1.30	0.77	0.62	1.05	3.46

Both pdfs for S_d^*/S_L and S_d^{*2D}/S_L exhibit finite probabilities of assuming negative values, especially for the flames with high values of Ka. A negative value of displacement speed indicates that the negative contribution of the molecular diffusion rate $\nabla\cdot(\rho D\nabla c)$ locally overcomes the positive contribution of $\dot{w}$ (see Eq. (2i)). This behaviour can be explained in terms of the scaling analysis of Peters [1] for unity Lewis number flames, which suggested that:

$$\frac{(S_r+S_n)}{\upsilon_\eta}\sim\frac{S_L}{\upsilon_\eta}\sim O\left(\frac{1}{\sqrt{Ka}}\right)\quad\text{and}\quad\frac{S_t}{\upsilon_\eta}\sim-\frac{2D\kappa_m}{\upsilon_\eta}\sim O(1) \tag{9}$$

where υ_η is the Kolmogorov velocity scale, and (S_r+S_n) and κ_m are taken to scale with S_L and the Kolmogorov length scale η respectively according to Peters [1]. The aforementioned scalings of combined reaction and normal diffusion component of displacement speed (S_r+S_n) and curvature κ_m were subsequently confirmed by DNS data [21]. Eq. (9) clearly suggests that in the thin reaction zones regime (i.e. $Ka>1$) the effects of (S_r+S_n) are likely to weaken progressively in comparison to the contribution of S_t with increasing Karlovitz number Ka [1]. This suggests that for large values of Karlovitz number the negative contribution of S_t can more readily overcome the predominantly positive contribution of (S_r+S_n) to yield a negative value of displacement speed S_d [1], which eventually gives rise to an increased probability of finding negative values of S_d for flames with increasing value of Karlovitz number Ka, as suggested by Fig. 3a–c. Negative values of estimated S_d^*/S_L have also been obtained by Hartung et al. [5] for turbulent premixed flames and negative values of S_d^*/S_L have also been experimentally reported by Heeger et al. [58] for turbulent edge flames. The physical interpretation and the mechanisms which could give rise to negative displacement speed is discussed in detail by Gran et al. [14] and interested readers are referred to Ref. [14] for further information. The non-zero probability of finding negative S_d^*/S_L is consistent with several previous DNS [13–21] studies. It can be seen from Fig. 3a–c that the probability of finding positive value of S_d^*/S_L supersedes the probability of obtaining negative values of S_d^*/S_L in all cases, which results in a positive mean value μ_{SD} for each individual cases (see Tables 3 and 4). The variation of mean values of $S_d^*=\rho S_d/\rho_0$ throughout the flame brush for statistically planar flames with unity Lewis number has been presented elsewhere and interested readers are referred to Refs. [19,23,25] where similar variations were observed for cases comparable to the present study. The mean values of S_d^*/S_L (i.e. μ_{SD}) for five different c isosurfaces across the flame brush at $t=\delta_{th}/S_L$ are presented in Table A1 in Appendix A.

It can be seen from Fig. 3a–c that the probability of finding high magnitudes of S_d^*/S_L remains smaller than for S_d^{*2D}/S_L and the peak value of S_d^{*2D}/S_L pdfs remains smaller than the S_d^*/S_L pdfs. This tendency is particularly prevalent for high u' cases (see cases D and E), whereas for small u' cases (see cases A and B) the difference between S_d^*/S_L and S_d^{*2D}/S_L pdfs remains negligible. However, the most probable values of both the normalised density-weighted displacement speed S_d^*/S_L and its two-dimensional counterpart S_d^{*2D}/S_L remain close to unity which is substantiated by the values of μ_{SD}^{2D}/μ_{SD} reported in Table 3 where μ_{SD}^{2D} is the mean value of S_d^{*2D}/S_L. However, the larger width of S_d^{*2D}/S_L pdfs compared to S_d^*/S_L pdfs leads to greater values for σ_{SD}^{2D} than for σ_{SD} (see Table 3), where σ_{SD}^{2D} is the standard-deviation of S_d^{*2D}/S_L. The values of μ_{SD}^{2D}/μ_{SD} and $\sigma_{SD}^{2D}/\sigma_{SD}$ halfway through the simulation (i.e. $t=0.5\delta_{th}/S_L$) are also presented in Table 4 for the $c=0.8$ isosurface, which showed μ_{SD}^{2D}/μ_{SD} remains close to unity whereas σ_{SD}^{2D} remains greater than σ_{SD}^{2D} since an early stage of flame–turbulence interaction. The observations made for the $c=0.8$ isosurface are also applicable for other c isosurfaces across the flame brush (see Table A1 in Appendix A).

To explain the differences between S_d^*/S_L and S_d^{*2D}/S_L pdfs it is instructive to examine the statistics of $|\cos\alpha|$. The pdfs of $|\cos\alpha|$ on the $c=0.8$ isosurface are shown in Fig. 4a which show a predominant probability of finding $|\cos\alpha|\approx 1$ for all cases, which indicates $\alpha=0^0$ is the most probable value of α. This can further be substantiated from the pdfs of $\left(N_1^2+N_2^2\right)$ on the $c=0.8$ isosurface (see Fig. 4b), which demonstrate overwhelming probability of finding $\left(N_1^2+N_2^2\right)\approx 1$ for all cases, which is consistent with previous findings [48,49]. This behaviour can be explained in terms of a curvature shape-factor s_h, which is defined as [48,49]: $s_h=h_{\min}/h_{\max}$, where $h_{\min}$ is the smaller of κ_1 and κ_2 by magnitude and $h_{\max}$ is the other. A value of $s_h=1$ corresponds to spherical curvature, $s_h=0$ to cylindrical curvature and $s_h=-1$ to spherical saddle points. Pdfs of s_h in Fig. 4c show that the probability of finding locally cylindrical structure is highest. There is a modest probability of finding spherical saddle points and zero probability of finding spherical curvature. There is little variation between different c isosurfaces. As the flame surface is predominantly cylindrically curved, the probability of finding $\left(N_1^2+N_2^2\right)\approx 1$ remains predominant throughout the flame surface. If the x_1-direction is taken to be the mean direction of flame propagation, the flame normal movement is predominantly aligned with x_1, and the directions x_2 and x_3 are expected to be statistically similar. This suggests that the pdfs of $\left(N_1^2+N_3^2\right)$ are going to be qualitatively similar to the pdfs of $\left(N_1^2+N_2^2\right)$, which is indeed found to be the case here but not shown here for the sake of brevity. In order to explain the above behaviour the pdfs of N_1 and N_2 on the $c=0.8$ isosurface are shown in Figs. 4d and e respectively for all the cases considered here. According to the definition of flame normal vector $\vec{N}=-\nabla c/|\nabla c|$ the flame normal points towards the unburned reactants. The component N_1 points predominantly to the mean direction of flame propagation, and from Fig. 4c it can be seen that whereas the mean direction of propagation is in the negative x_1-direction there is a finite probability of finding positive values of N_1, i.e. the flame locally may face backwards. Due to flame wrinkling the peak of the pdf of N_1 for some c isosurfaces is shifted from -1 to a slightly less negative value indicating the extent of the deformation from a planar flame sheet. The pdfs of the transverse components N_2 and N_3 are similar to one another since the x_2 and x_3 directions are statistically identical, and thus the pdf of N_3 is not separately shown and the transverse components vary over the full range of -1 to 1 depending on the extent of the local wrinkling of the flame surface (see Fig. 4e). In a statistically planar flame with mean direction of flame propagation aligned with the x_1-direction, it is extremely rare to find $|N_2|=1$ and $|N_3|=1$ (i.e. a situation where the flame normal is locally aligned exactly along the either x_2 or x_3 direction). Hence, the probabilities of finding $N_1=0$ or $|N_2|=1$ and $|N_3|=1$ are close to zero for the cases considered here (see Fig. 4d and e). However, there is a non-negligible probability of finding N_2 and N_3 with magnitudes close to unity (see Fig. 4e) which in turn gives rise to negligible magnitudes of N_1 (see Fig. 4d). The behaviour of the flame normal components is consistent with previous DNS [49] and experimental results [59,60].

The contours of joint pdf between N_1 and N_2 for case D are presented in Fig. 5a where the arc of a circle of unit radius is evident. The same is true for the joint pdf of N_1 and N_3 which can be seen in Fig. 5b as N_2 and N_3 are statistically similar to each other and the slight difference between the differences in Fig. 5a and b arise due to finite sample size. On a given c isosurface $N_1^2+N_2^2+N_3^2=1$, but if N_1 remains close to -1 in most locations the equation $N_2^2+N_3^2=\varepsilon^2$ holds where ε is a small number. This suggests that N_2 and N_3 will fall on the circumference of circles of different diameters corresponding to different values of N_1. This is illustrated by the joint pdf between N_2 and N_3 as shown in Fig. 5c which produces a filled-in circle of unit radius. The incomplete filling of the circle is due to the finite sample size. It is possible to obtain non-zero (but negligible) probability of finding $|N_2|=1$ or $|N_3|=1$ and $N_1=0$ for infinite sample size but this situation is not encountered here because of the finite sample size. It is important to note that

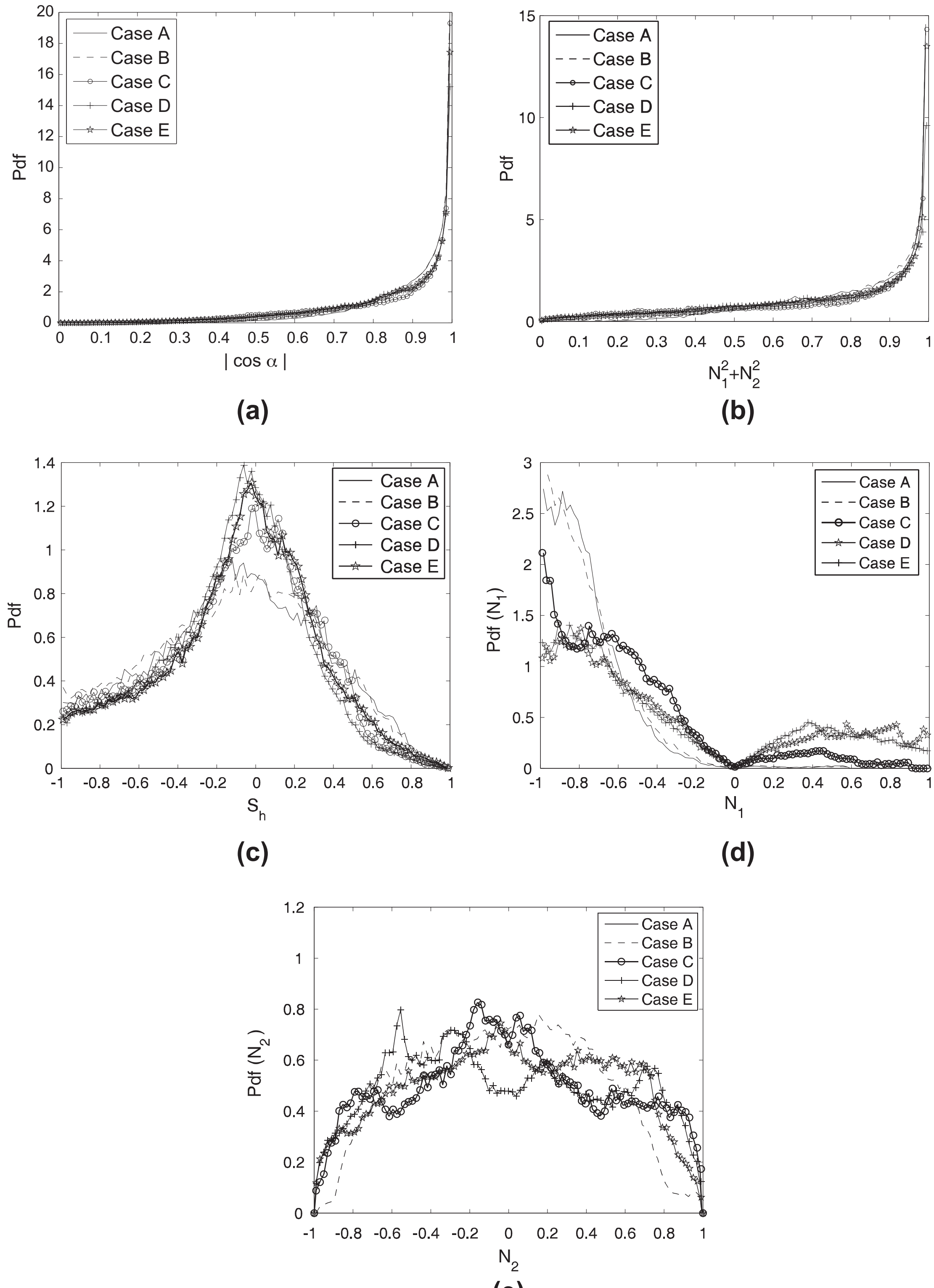

Fig. 4. Pdfs of (a) $|\cos\alpha|$; (b) $N_1^2+N_2^2$; (c) shape-factor s_h; (d) N_1 and (e) N_2 on the $c = 0.8$ isosurface for all cases.

$N_1^2+N_3^2=1$ when $N_2^2/\left(N_2^2+N_3^2\right)=0$, indicating that the local flame surface has cylindrical structure with axis aligned in the x_2 direction. Similarly, cylindrical structure with axis aligned in the x_3 direction is obtained when $N_1^2+N_2^2=1$ and $N_2^2/\left(N_2^2+N_3^2\right)=1$. This explains why the pdfs of $N_1^2+N_2^2$ and $N_1^2+N_3^2$ are each peaked at unity, and why a part of the circular arc of unit radius is obtained in the joint pdfs of N_1 and N_2 (Fig. 5a) and N_1 and N_3 (Fig. 5b). Although the joint pdfs are shown only for case D in Fig. 5, the same qualitative behaviour has been observed in other cases. These results, taken together with the results for curvature shape factor (Fig. 4c), indirectly prove the overwhelming presence of cylindrical structure on a three-dimensional wrinkled flame surface.

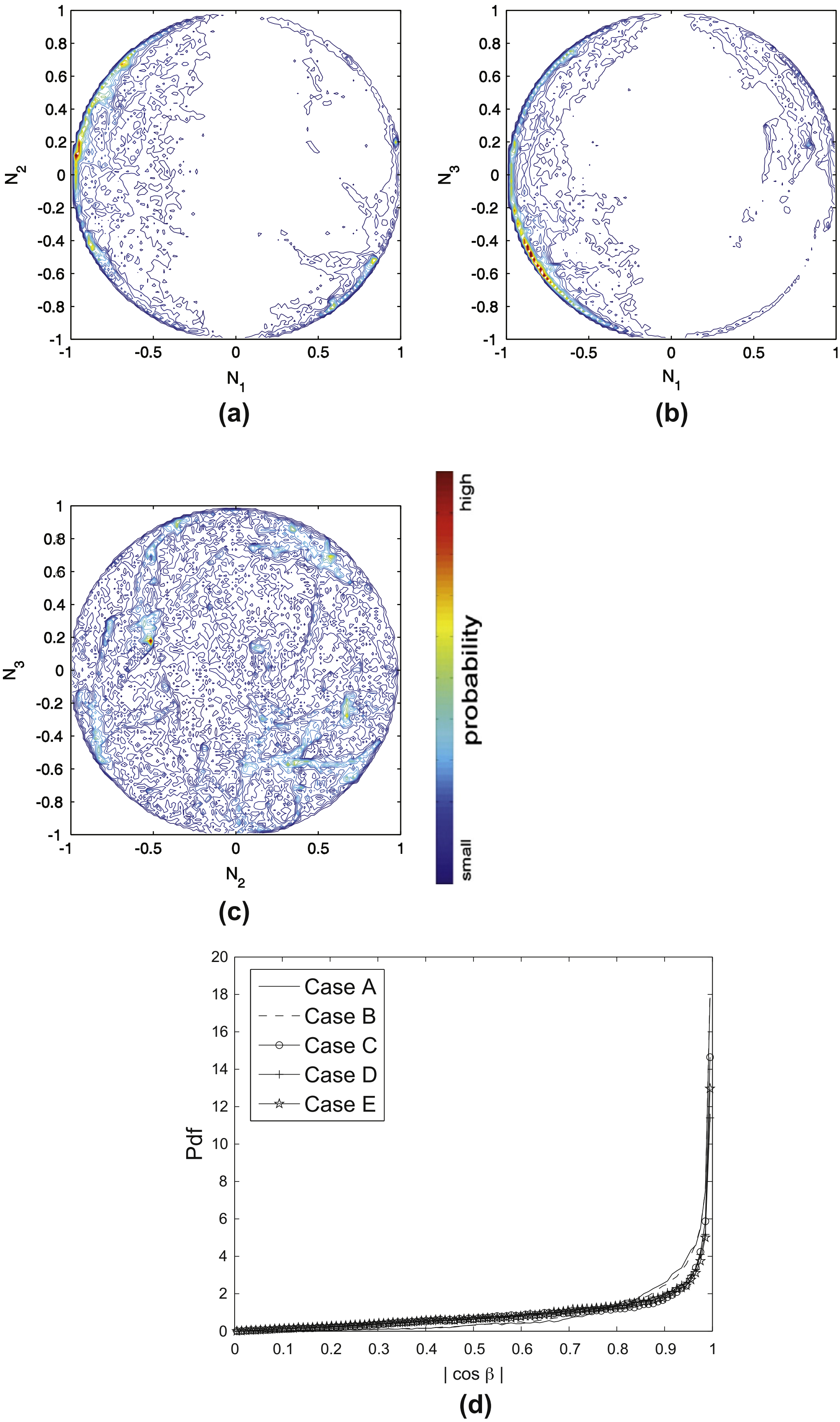

Fig. 5. Contours of joint pdfs for pairs of normal vector components evaluated on the $c = 0.8$ isosurface: (a) N_1 and N_2; (b) N_1 and N_3; (c) N_2 and N_3 for case D. (e) Pdfs of $|\cos\beta|$ on the $c = 0.8$ isosurface for all cases.

The predominant probability of finding $\left(N_1^2+N_3^2\right)\approx 1$ suggests overwhelming probability of finding $|\cos\beta|\approx 1$ where $|\beta|$ is given by $\cos^{-1}|\vec{N}^{2D}.\vec{M}|$ where $\vec{N}^{2D}$ is the apparent flame normal vector in two-dimensional projection and $\vec{M}$ is the unit vector in the direction of mean flame propagation (i.e. x_1-direction). Hartung et al. [5] approximated $|\cos\alpha|$ by $|\vec{N}_{2D}\cdot\vec{M}|=|\cos\beta|$ (i.e. $|\cos\alpha|$ = $|\cos\beta|$). The pdfs of $|\cos\beta|$ on the c = 0.8 isosurface are shown in Fig. 5d, which show a predominant probability of finding $|\cos\beta|\approx 1$ for all cases. Comparing Figs. 4a and 5d, it is evident that the pdfs of $|\cos\alpha|$ can be adequately captured by $|\cos\beta|$ as assumed by Hartung et al. [5]. The probability of finding non-unity values of $|\cos\alpha|$ and $|\cos\beta|$ increases with increasing u' due to the larger extent of flame wrinkling (see Fig. 2a–e).

As $\cos\alpha$ appears explicitly in the expression for S_d^{2D}, the values of $\cos\alpha$ are more relevant to this investigation than the magnitude of the angle α. Moreover, $|\cos\alpha|$ is modelled by $|\cos\beta|$ for the purpose of evaluating S_d^{*2D} as discussed in detail by Hartung et al. [5] so $|\cos\beta|$ is the quantity of interest. Thus the pdfs of $|\alpha|$ and $|\beta|=\cos^{-1}|\vec{N}^{2D}.\vec{M}|$ are not shown here for the sake of brevity. However, it is clear from Figs. 4a and 5d that the probability of finding negligible magnitude of α and β (i.e. $|\cos\alpha|\approx 1$ and $|\cos\beta|\approx 1$) is predominant for all cases. By contrast the probability of obtaining the magnitudes of α and β close to $\pi/2$ (i.e. $|\cos\alpha|$ = 0 and $|\cos\beta|$ = 0) is negligible for all cases.

The predominant probability of finding $|\cos\alpha|\approx 1$ and zero probability of finding $|\cos\alpha|$ = 0 in Fig. 4a indicates that the singularity in Eq. (5) when $\cos\alpha$ = 0 is never encountered for all the cases considered here. This is a consequence of the fact that S_d^{*2D} is evaluated here on a measurement plane which contains the mean direction of flame propagation (i.e. x_1-direction). It is clear that it is beneficial to choose a measurement plane which contains the mean flame propagation direction to obtain meaningful S_d^{*2D} statistics. A randomly or inadequately chosen two-dimensional measurement plane may increase the probability of finding $\cos\alpha$ = 0 leading to unphysical results for S_d^{*2D}.

Based on the above discussion, it is clear that the large probability of finding $\cos\alpha$ = 1 (or $\alpha = 0^0$) in the low u' cases (e.g. cases A and B) ultimately gives rise the pdfs of two-dimensional projection of density-weighted displacement speed S_d^{*2D}/S_L, which are similar to the S_d^*/S_L pdfs because the contribution of $u_3\tan\alpha$ is likely to be negligible in these cases ($\because \tan\alpha\approx 0$). However, for high values of u' (e.g. cases D and E), the probability of finding $|\cos\alpha|\neq 1$ remains relatively greater than in cases A and B which acts to produce a larger spread of S_d^{*2D}/S_L values than for S_d^*/S_L according to Eq. (5), as $\cos\alpha$ < 1. Moreover, greater probability of finding $|\cos\alpha|\neq 1$ in cases D and E also leads to non-negligible effects of $u_3\tan\alpha$ on the range of values obtained for S_d^{*2D}/S_L. As a large range of local u_3 values are obtained for higher u' cases, the contribution of u_3 $\tan\alpha$ also contributes to the spreading of two-dimensional projection of density-weighted displacement speed S_d^{*2D}/S_L. In the present case, the mean value of u_3 remains almost equal to zero and thus the contribution of $u_3\tan\alpha$ does not affect the mean value of S_d^{*2D}/S_L. However, the contribution of $u_3\tan\alpha$ is likely to contaminate the mean value of S_d^{*2D}/S_L for non-zero mean values of u_3. The foregoing discussion suggests that pdfs of two-dimensional projection of density-weighted displacement speed S_d^{*2D}/S_L are an accurate reflection of actual three-dimensional density-weighted displacement speed S_d^*/S_L pdfs for small values of u' when $|\cos\alpha|$ predominantly assumes a value of unity. However, often in engineering applications the value of turbulent Reynolds number $\mathrm{Re}_t\sim(u'/S_L)^4/Ka^2$ attains much greater value than the flames considered in the present study for the purpose of computational economy of DNS simulations. The scaling $u'/S_L\sim\mathrm{Re}_t^{1/4}Ka^{1/2}$ suggests that for large values of turbulent Reynolds number the probability of finding $|\cos\alpha|\neq 1$ will increase and $u_3\tan\alpha$ will have a non-negligible effect on the range of values obtained for S_d^{*2D}/S_L. This situation will be further aggravated in the thin reaction zones regime due to high values of Karlovitz number Ka. This demonstrates that the pdf of S_d^{*2D} provides a reasonably accurate measure of the true three-dimensional displacement speed only for small values of u'/S_L and Re_t but this may not be true for higher values of turbulent Reynolds number Re_t. Further analysis in this regard will be necessary.

5.3. Comparison between S_t^* and S_t^{*2D} pdfs

It is evident from Eqs. (4) and (7) that S_t^{*2D} can only accurately predict S_t^* if the statistical behaviour of two-dimensional curvature κ_m^{2D} faithfully captures the statistical behaviours of three dimensional curvature κ_m. The pdfs of κ_m and κ_m^{2D} on the c = 0.8 isosurface for cases A, C and E are shown in Fig. 6a–c respectively and the pdfs of curvatures κ_m and κ_m^{2D} in cases B and D are qualitatively similar to the cases A and E respectively and thus are not shown here for the sake of brevity. The same qualitative behaviour has been observed for other c-isosurfaces. Figure 6a–c shows that the pdfs of κ_m and κ_m^{2D} show almost equal probability of finding positive and negative values and the most probable value remains close to the zero value, as all the flames are statistically planar in nature. Comparing Fig. 6a–c indicates that the probability of finding large magnitude of κ_m is greater than the probability of finding large κ_m^{2D} magnitudes. These observations are found to be consistent with previous two-dimensional and three-dimensional curvature pdf comparisons by Gashi et al. [50]. This suggests the pdfs of two-dimensional projection of tangential-diffusion component of density-weighted displacement speed $S_t^{*2D}=-2\rho D\kappa_m^{2D}/\rho_0$ are going to be narrower than the pdfs of its actual three-dimensional counterpart $S_t^*=-2\rho D\kappa_m/\rho_0$ and the standard-deviation of S_t^{*2D} is likely to be smaller than the standard-deviation of S_t^*. However, the mean values of S_t^{*2D} and S_t^* for statistically planar flames are likely to be close to zero as the mean values of κ_m and κ_m^{2D} remain close to zero.

It has been shown earlier that premixed flames locally show a dominant probability of finding cylindrical curvature. Thus, if a plane obliquely cuts a cylindrical surface, the projected radius of curvature on the plane is going to be greater than the actual radius of curvature. This leads to smaller magnitudes in curvature in the obliquely intersecting plane than the actual curvature, as curvature is inversely proportional to the radius of curvature. This ultimately leads to wider pdfs of κ_m than the pdfs of κ_m^{2D}. It has been found here that scaling two-dimensional curvature as $\kappa_m^*=\pi\times\kappa_m^{2D}/2$ successfully captures the pdfs of κ_m for all cases in spite of large variations of Da, Ka and Re_t (see Table 1), as demonstrated in Fig. 6a–c. Similar behaviour has been observed for other c-isosurfaces. Furthermore this suggests that pdfs of $\pi\times S_t^{*2D}/2$ also successfully capture the pdfs of S_t^* (see Eqs. (4) and (7)), as demonstrated in Fig. 7a–c for cases A, C and E respectively. Similar results have been obtained for cases B and D, which are not presented here for the sake of brevity. It can further be seen from Tables 3 and A1 in Appendix A that the standard-deviation of $\pi\times S_t^{*2D}/2$ (i.e. $\pi/2\times\sigma_{ST}^{2D}$) remains of the same order of the standard-deviation of S_t^* (i.e. σ_{ST}) for all the cases considered here when the statistics were extracted (i.e. $t=\delta_{th}/S_L$). Similar behaviour has also been observed halfway through the simulation (i.e. $t=0.5\delta_{th}/S_L$) as can be seen from Table 4. In this regard, it is worth noting that Hawkes et al. [36] recently obtained an analytical relation between the three-dimensional surface averaged curvature $\overline{(\kappa_m)}_s=\overline{\kappa_m|\nabla c|}/\Sigma_{gen}$ and its two-dimensional counterpart $\overline{(\kappa_m^{2D})}_s=\overline{\kappa_m|\nabla c|^{2D}}/\overline{|\nabla c|^{2D}}$ in the context of RANS in the following manner: $\overline{(\kappa_m)}_s=\pi/2\times\overline{(\kappa_m^{2D})}_s$ based on the assumption of isotropy of the flame normal vector where $|\nabla c|^{2D}$ is the magnitude of the reaction progress variable gradient in the two-dimensional

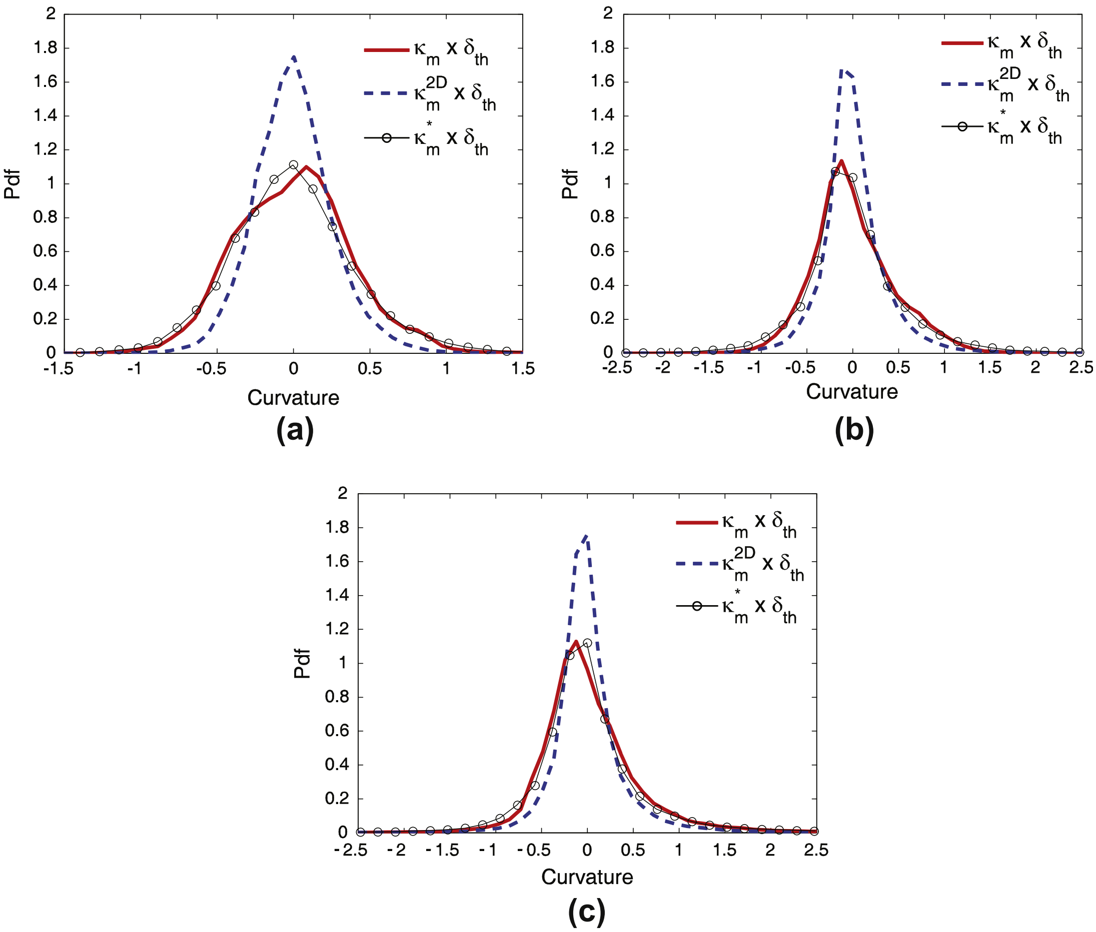

Fig. 6. Pdfs of $\kappa_m \times \delta_{th}$; $\kappa_m^{2D} \times \delta_{th}$ and $\kappa_m^{2D} \times \delta_{th} \times (\pi/2)$ on the $c = 0.8$ isosurface for cases: (a) A; (b) C; (c) E.

projection (e.g. in the context of Fig. 1a $|\nabla c|^{2D}$ is given by: $|\nabla c|^{2D} = \sqrt{(\partial c/\partial x_1)^2 + (\partial c/\partial x_2)^2}$). Although the correction factor $\pi/2$ relates $\overline{(\kappa_m)}_s$ and $\overline{(\kappa_m^{2D})}_s$ as found by theoretical analysis, the use of this constant correct factor to obtain the pdfs of κ_m from the pdfs of κ_m^{2D} is empirical in nature and a deeper analysis will be required to justify this factor. It is worth noting that the mean values of κ_m and κ_m^{2D} remain close to zero in statistically planar flames and no correction factor is necessary to relate the mean values of κ_m and κ_m^{2D}.

5.4. Comparison between $(S_r^* + S_n^*)$ and $(S_r^* + S_n^*)^{2D}$ pdfs

The pdfs of combined reaction and normal diffusion component of density-weighted displacement speed (normalised) $(S_r^* + S_n^*)/S_L$ and its two-dimensional counterpart (i.e. $(S_r^* + S_n^*)^{2D}/S_L = S_d^{*2D}/S_L - S_t^{*2D}/S_L = S_d^{*2D}/S_L + 2\rho D\kappa_m^{2D}/\rho_0 S_L$) on the $c = 0.8$ isosurface for cases A, C and E are shown Fig. 8a–c respectively. The cases B and D are shown here for conciseness as these cases exhibit same qualitative behaviours as that of cases A and E respectively. Comparing density-weighted displacement speed S_d^*/S_L and combined reaction and normal diffusion component of density-weighted displacement speed $(S_r^* + S_n^*)/S_L$ pdfs from Figs. 3a–c and 8a–c, it is evident that the probability of finding negative values is relatively smaller for $(S_r^* + S_n^*)/S_L$ than S_d^*/S_L, which suggests that the negative value of S_d^*/S_L principally originates due to S_t^*/S_L, which is consistent with scaling arguments proposed by Peters [1] for the thin reaction zones regime. Tables 3 and A1 indicate that the standard-deviation of $(S_r^* + S_n^*)/S_L$ (i.e. σ_{SRN}) is smaller than the standard-deviation of S_d^*/S_L (i.e. σ_{SD}) and σ_{SRN} increases with increasing u'. In turbulent flames, wrinkling leads to a large range of curvature and S_t^* variations (see Eq. (4)) which makes S_d^*/S_L pdfs wider than corresponding $(S_r^* + S_n^*)/S_L$ pdfs. This ultimately leads to a greater value of σ_{SD} than σ_{SRN}. Moreover, the pdfs of combined reaction and normal diffusion component of density-weighted displacement speed $(S_r^* + S_n^*)/S_L$ for all cases suggest that the most probable value of $(S_r^* + S_n^*)/S_L$ remains about unity. This leads to a mean value of normalised combined reaction and normal diffusion component of density-weighted displacement speed $(S_r^* + S_n^*)/S_L$ close to unity (i.e. $\mu_{SRN} \approx 1$), (see Tables 3 and A1). Figure 8a–c indicate that the pdfs of $(S_r^* + S_n^*)^{2D}/S_L$ are wider than the $(S_r^* + S_n^*)/S_L$ pdfs and thus the standard-deviation of $(S_r^* + S_n^*)^{2D}/S_L$ remains greater than that of $(S_r^* + S_n^*)/S_L$ although the most probable and mean values of $(S_r^* + S_n^*)^{2D}/S_L$ remain of the order of unity. This can be substantiated from the values of μ_{SRN}^{2D}/μ_{SRN} and $\sigma_{SRN}^{2D}/\sigma_{SRN}$ at $t = \delta_{th}/S_L$ presented in Table 3 for the $c = 0.8$ isosurface where μ_{SRN}^{2D} and σ_{SRN}^{2D} are the mean and standard-deviations of $(S_r^* + S_n^*)^{2D}/S_L$ respectively. A similar qualitative behaviour has been observed for other c isosurfaces across the flame brush (see Table A1 in Appendix A). It can be also be seen from Table 4 that μ_{SRN}^{2D}/μ_{SRN} remains close to unity and σ_{SRN}^{2D} remains significantly greater than σ_{SRN} since $t = 0.5\delta_{th}/S_L$ although μ_{SRN}^{2D} assumes values smaller than unity but close to unity due to the developing nature of flame–turbulence interaction.

As the pdfs of S_d^{*2D}/S_L are wider than S_d^*/S_L (see Fig. 3a–c) and the pdfs of S_t^{*2D}/S_L are narrower than S_t^*/S_L (see Fig. 7a–c), the pdfs of $(S_r^* + S_n^*)^{2D}/S_L$ turn out to be wider than the pdfs of $(S_r^* + S_n^*)/S_L$. Although the pdfs of $\pi \times S_t^{*2D}/2S_L$ successfully mimic the pdfs of

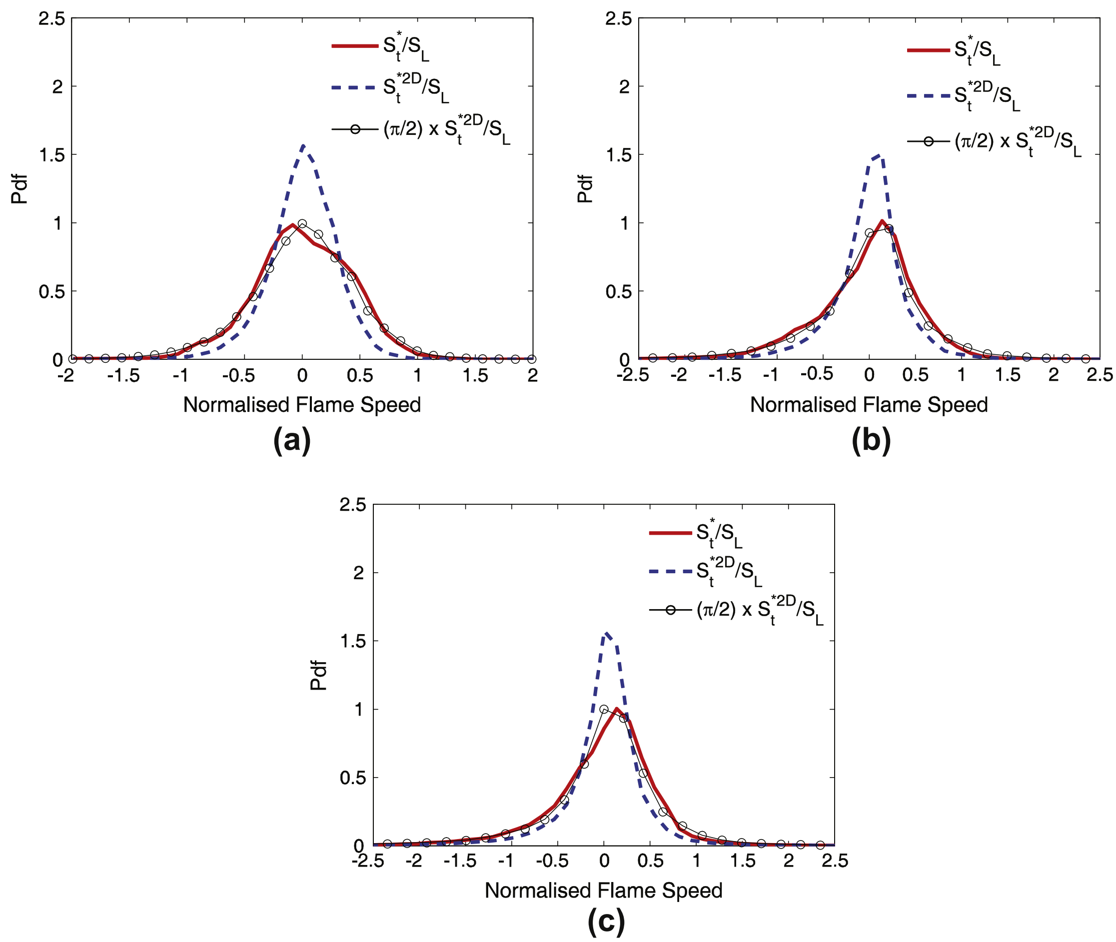

Fig. 7. Pdfs of S_t^*/S_L; S_t^{*2D}/S_L and $S_t^{*2D}/S_L \times (\pi/2)$ on the $c = 0.8$ isosurface for cases: (a) A; (b) C; (c) E.

S_t^*/S_L, the pdfs of $S_d^{*2D}/S_L - (\pi/2) \times S_t^{*2D}/S_L = S_d^{*2D}/S_L + 2\rho D\kappa_m^{2D}/\rho_0 S_L \times \pi/2$ remain comparable to the pdfs of the two-dimensional counterpart of the combined reaction and normal diffusion component of density-weighted displacement speed $(S_r^* + S_n^*)^{2D}/S_L$ for all cases. This suggests that the correction for obtaining S_t^*/S_L from S_t^{*2D}/S_L is not sufficient to mimic $(S_r^* + S_n^*)/S_L$ pdfs from two-dimensional projection even for low u' cases (e.g. cases A) despite the fact that in these cases the pdfs of S_d^{*2D}/S_L remain almost similar to the S_d^*/S_L pdfs (see Fig. 3a). This suggests that although the distributions of $\pi \times S_t^{*2D}/2S_L$ remain comparable to that of S_t^*/S_L, the local three-dimensional curvature κ_m information cannot be adequately captured by just multiplying the two-dimensional curvature κ_m^{2D} by a constant multiplier (e.g. $\pi/2$) as done in the context of approximating κ_m pdfs from the pdfs of κ_m^{2D} (see Fig. 6a–c). This issue can further be elucidated by comparing actual curvature dependence of S_d^*/S_L and $(S_r^* + S_n^*)/S_L$ with κ_m^{2D} dependences of S_d^{*2D}/S_L and $(S_r^* + S_n^*)^{2D}/S_L$.

5.5. The local curvature dependence of displacement speed in two and three-dimensions

The contours of the joint pdf between normalised density-weighted displacement speed S_d^*/S_L and normalised curvature $\kappa_m \times \delta_{th}$ on the $c = 0.8$ isosurface for case C are shown in Fig. 9a, which show that S_d^*/S_L and $\kappa_m \times \delta_{th}$ are negatively correlated, consistent with several previous studies [13–21,23–29]. The same qualitative behaviour has been observed for other c isosurfaces across the flame brush for all cases, and this can be substantiated from the correlation-coefficients reported in Tables 5 and A2 (in Appendix A) at time $t = \delta_{th}/S_L$. This indicates that the correlation-coefficient between S_d^*/S_L and $\kappa_m \times \delta_{th}$ decreases with increasing u' for a given value of either Da or Ka, which is also consistent with earlier findings [18,20]. The correlation coefficients between S_d^*/S_L and $\kappa_m \times \delta_{th}$ at $t = 0.5\delta_{th}/S_L$ are also reported in Table 6 which show the same qualitative behaviour as observed at time $t = \delta_{th}/S_L$ (compare Tables 5 and 6). Figure 9a and Tables 5, 6 and A2 demonstrate that the correlation between S_d^*/S_L and $\kappa_m \times \delta_{th}$ is non-linear in nature. As the tangential-diffusion component of density-weighted displacement speed S_t^*/S_L and curvature $\kappa_m \times \delta_{th}$ are predictably negatively correlated with a correlation coefficient equal to -1 (see Eq. (4)), the non-linearity of the correlation between S_d^*/S_L and $\kappa_m \times \delta_{th}$ is induced by the curvature κ_m dependence of combined reaction and normal diffusion component $(S_r^* + S_n^*)$. This is evident from the contours of joint pdf between $(S_r^* + S_n^*)/S_L$ and $\kappa_m \times \delta_{th}$ on the $c = 0.8$ isosurface for case C, as shown in Fig. 9b, which exhibits a non-linear correlation with both positive and negative correlating branches but the net correlation remains weak. Same qualitative behaviour has been observed for other c isosurfaces across the flame brush (see Table A2 in Appendix A). Tables 5 and 6 suggest that the same qualitative behaviour is observed for other cases since $t = 0.5\delta_{th}/S_L$. The physical explanation behind the positive and negative correlating branches in the joint pdf between the combined reaction and normal diffusion component of displacement speed $(S_r^* + S_n^*)/S_L$ and $\kappa_m \times \delta_{th}$ has been provided elsewhere in detail [19–21,23–28] and thus will not be repeated here for the sake of brevity. Fig. 9a and b indicates the negative correlation between S_t^* and κ_m is principally responsible for the

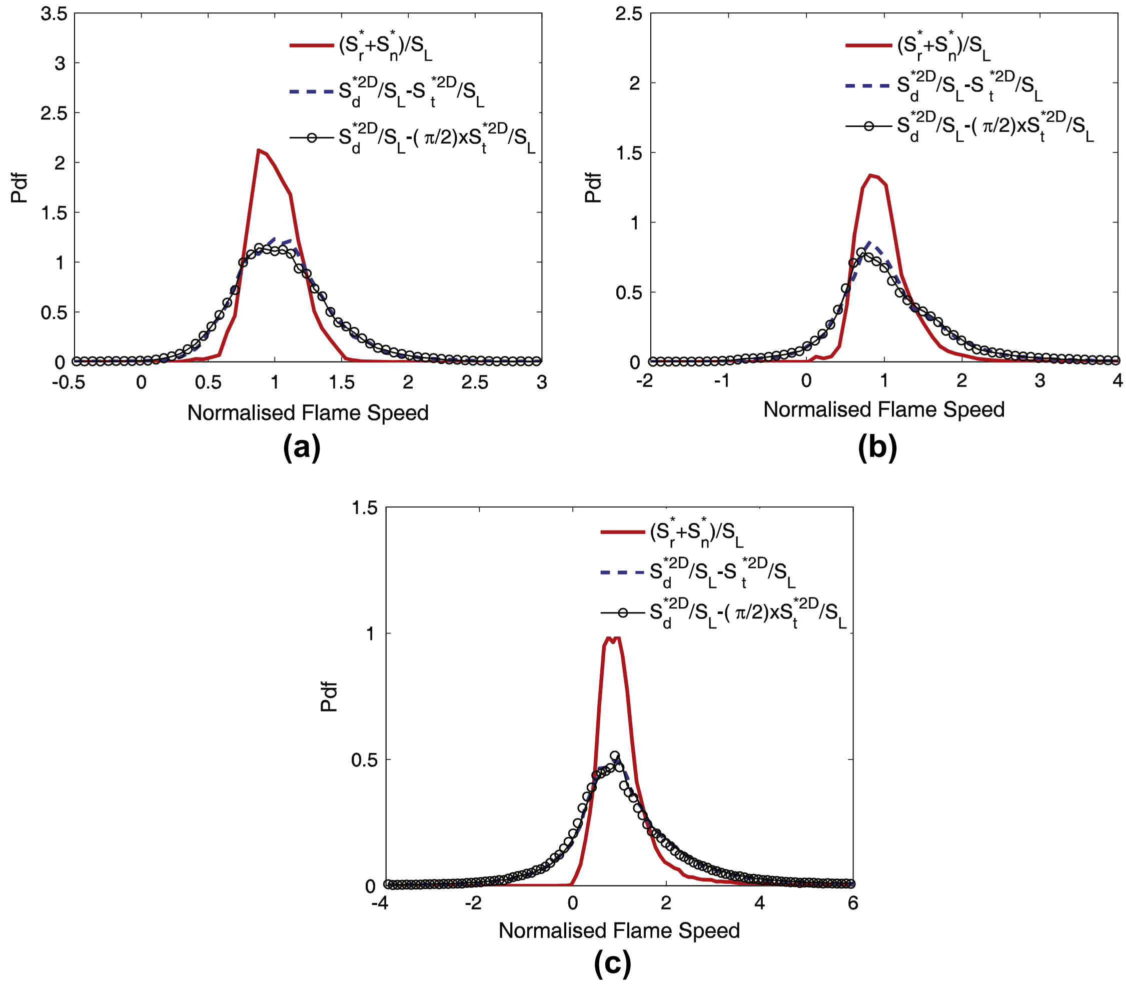

Fig. 8. Pdfs of $(S_r^*+S_n^*)/S_L$; $(S_r^*+S_n^*)^{2D}/S_L = S_d^{*2D}/S_L - S_t^{*2D}/S_L = S_t^{*2D}/S_L + 2\rho D\kappa_m^{2D}/\rho_0 S_L$ and $S_d^{*2D}/S_L - (\pi/2) \times S_t^{*2D}/S_L = S_d^{*2D}/S_L + 2\rho D\kappa_m^{2D}/\rho_0 S_L \times \pi/2$ on the $c = 0.8$ isosurface for cases: (a) A; (b) C; (c) E.

negative correlation between S_d^*/S_L and $\kappa_m \times \delta_{th}$. The contours of the joint pdfs between S_d^{*2D}/S_L and $\kappa_m^{2D} \times \delta_{th}$ and between two-dimensional projection of combined reaction and normal diffusion component of density-weighted displacement speed (i.e. $(S_r^*+S_n^*)^{2D}/S_L = S_d^{*2D}/S_L - S_t^{*2D}/S_L = S_d^{*2D}/S_L + 2\rho D\kappa_m^{2D}/\rho_0 S_L)$ and two-dimensional curvature $\kappa_m^{2D} \times \delta_{th}$ on the $c = 0.8$ isosurface for case C are shown in Fig. 9c and d respectively. Comparison between Fig. 9a with c reveals that the correlation between S_d^{*2D}/S_L and $\kappa_m^{2D} \times \delta_{th}$ turns out to be much weaker than the correlation between S_d^{*2D}/S_L and $\kappa_m^{2D} \times \delta_{th}$, which is summarised in terms of correlation-coefficients in Tables 5 and 6 at times $t = \delta_{th}/S_L$ and $t = 0.5 \times \delta_{th}/S_L$ respectively. The correlation coefficients between S_d^{*2D}/S_L and $\kappa_m^{2D} \times \delta_{th}$ for other c isosurfaces across the flame brush at time $t = \delta_{th}/S_L$ are presented in Table A2 in Appendix A which substantiates that correlation between S_d^{*2D}/S_L and $\kappa_m^{2D} \times \delta_{th}$ remains much weaker than the correlation between S_d^{*2D}/S_L and $\kappa_m^{2D} \times \delta_{th}$ throughout the flame brush. Figure 9d shows the net correlation between $(S_r^*+S_n^*)^{2D}/S_L$ and $\kappa_m^{2D} \times \delta_{th}$ remains weak (see Table 5) but this correlation does not show any clear positive and negative correlating branches and thus remains qualitatively different from the correlation between $(S_r^*+S_n^*)/S_L$ and $\kappa_m \times \delta_{th}$. In order to explain this behaviour the contours of joint pdfs between S_d^{*2D}/S_L and S_d^*/S_L on the $c = 0.8$ isosurface for cases A, C and E are shown Fig. 10a–c respectively. The cases B and D are not explicitly shown for their similarity to cases A and E respectively. It is evident from Fig. 10a–c that S_d^{*2D}/S_L and S_d^*/S_L remain positively correlated with each other for all the cases but the scatter of the data around the line indicating the correlation coefficient equal to unity increases with increasing $u'/S_L \sim \mathrm{Re}_t^{1/4}Ka^{1/2}$, which indicates that the local behaviour of S_d^{*2D}/S_L is likely to be different from S_d^*/S_L for flames with high values of turbulent Reynolds number Re_t and Karlovitz number Ka. This can further be substantiated from Tables 5 and 6 that the correlation coefficients between S_d^{*2D}/S_L and S_d^*/S_L remain smaller than unity and the correlation-coefficients are generally smaller for high values of u' (compare cases A and B with cases D and E). A similar behaviour has been observed for other c isosurfaces across the flame brush (see Table A2). The contours of the joint pdfs between κ_m^{2D} and κ_m on the $c = 0.8$ isosurface for cases A, C and E are shown Fig. 10d–f respectively. The cases B and D are not explicitly shown for their similarity to cases A and E respectively. It is evident from Fig. 10d–f that κ_m^{2D} and κ_m remain positively correlated with each other and the scatter of data around the line indicating the correlation coefficient equal to unity remains considerable for all the cases. As a result of this, the correlation-coefficient between κ_m^{2D} and κ_m also remains smaller than unity for all cases (see Tables 5 and 6). A similar behaviour has been observed for other c isosurfaces across the flame brush (see Table A2). This suggests that the local variations of S_d^{*2D}/S_L, $(S_r^*+S_n^*)^{2D}/S_L$ and κ_m^{2D} are fundamentally different from the variations of S_d^*/S_L, $(S_r^*+S_n^*)/S_L$ and κ_m respectively, which leads to the difference between $(S_r^*+S_n^*)^{2D} - \kappa_m^{2D}$ and $(S_r^*+S_n^*) - \kappa_m$ and between $S_d^{*2D} - \kappa_m^{2D}$ and $S_d^* - \kappa_m$ correlations. As S_d^{*2D} and

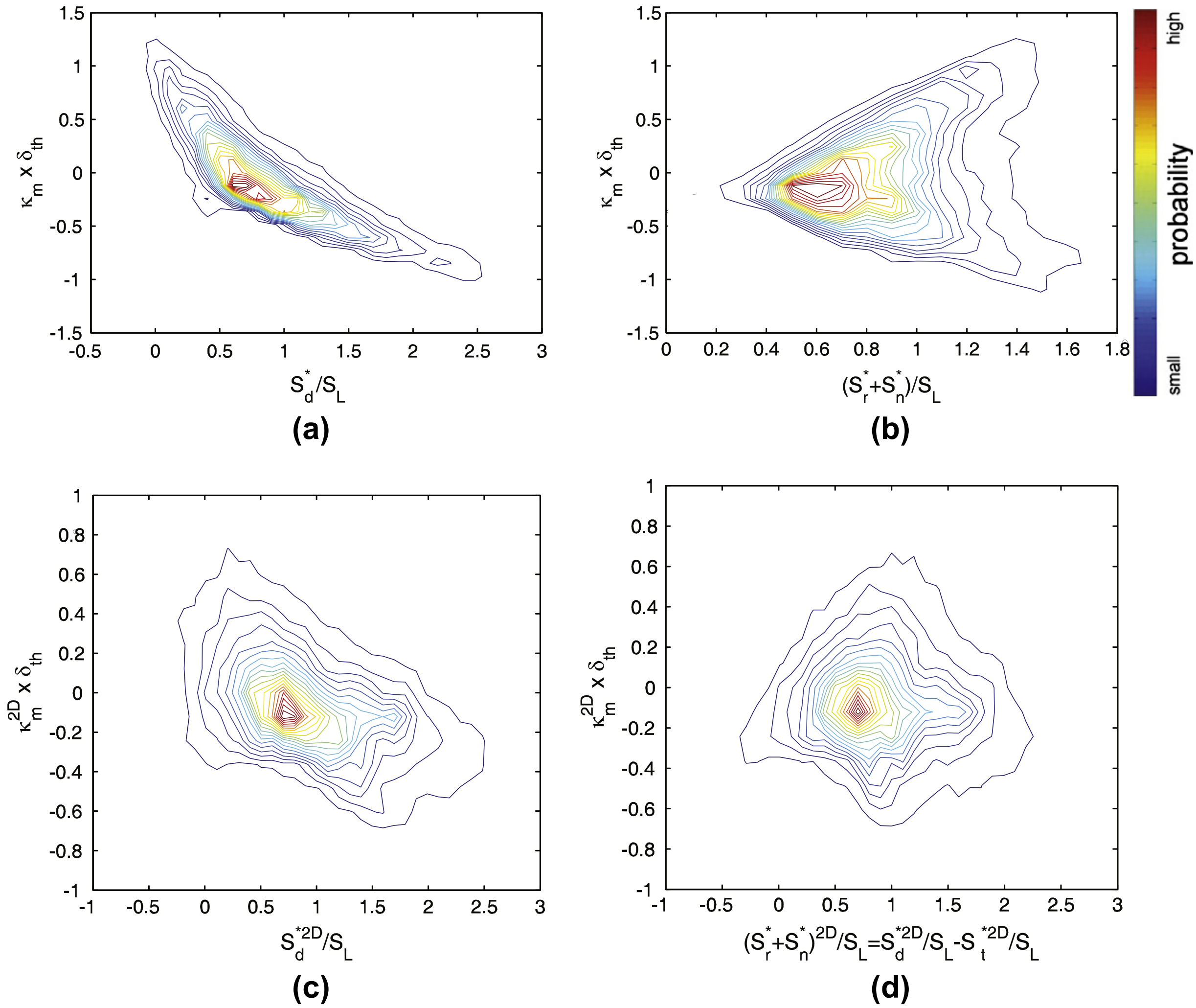

Fig. 9. Contours of joint pdf between (a) S_d^*/S_L and $\kappa_m \times \delta_{th}$; (b) $(S_r^* + S_n^*)/S_L$ and $\kappa_m \times \delta_{th}$; (c) S_d^{*2D}/S_L and $\kappa_m^{2D} \times \delta_{th}$ and (d) $(S_r^* + S_n^*)^{2D}/S_L = S_d^{*2D}/S_L - S_t^{*2D}/S_L = S_t^{*2D}/S_L + 2\rho D\kappa_m^{2D}/\rho_0 S_L$ and $\kappa_m^{2D} \times \delta_{th}$ on the $c = 0.8$ isosurface for case C.

Table 5
The relevant values of correlation-coefficients on the $c = 0.8$ isosurface when statistics were extracted (i.e. $t_{sim} = \delta_{th}/S_L$).

Case	$S_d^* - \kappa_m$	$(S_r^* + S_n^*) - \kappa_m$	$S_d^{*2D} - \kappa_m^{2D}$	$(S_r^* + S_n^*)^{2D} - \kappa_m^{2D}$	$S_d^* - S_d^{*2D}$	$\kappa_m - \kappa_m^{2D}$
A	−0.89	0.28	−0.59	0.025	0.89	0.80
B	−0.90	0.22	−0.60	0.022	0.89	0.78
C	−0.80	0.054	−0.35	0.075	0.73	0.69
D	−0.62	0.14	−0.10	0.16	0.50	0.68
E	−0.70	−0.053	−0.18	0.068	0.55	0.72

Table 6
The relevant values of correlation-coefficients on the $c = 0.8$ isosurface halfway through the simulation (i.e. $t = 0.5\delta_{th}/S_L$).

Case	$S_d^* - \kappa_m$	$(S_r^* + S_n^*) - \kappa_m$	$S_d^{*2D} - \kappa_m^{2D}$	$(S_r^* + S_n^*)^{2D} - \kappa_m^{2D}$	$S_d^* - S_d^{*2D}$	$\kappa_m - \kappa_m^{2D}$
A	−0.86	0.29	−0.56	0.033	0.87	0.78
B	−0.86	0.28	−0.54	0.055	0.87	0.78
C	−0.76	0.051	−0.32	0.068	0.68	0.75
D	−0.78	0.20	−0.15	0.104	0.42	0.77
E	−0.74	−0.053	−0.13	0.140	0.43	0.78

κ_m^{2D} are not perfectly correlated with S_d^* and κ_m respectively and the contribution of $u_3 \tan\alpha$ is unlikely to be dependent on κ_m^{2D}, the two-dimensional displacement speed S_d^{*2D} is found to be weakly correlated with κ_m^{2D}.

6. Conclusions

In a recent paper, Hartung et al. [5] presented an experimental methodology for obtaining two-dimensional projection of

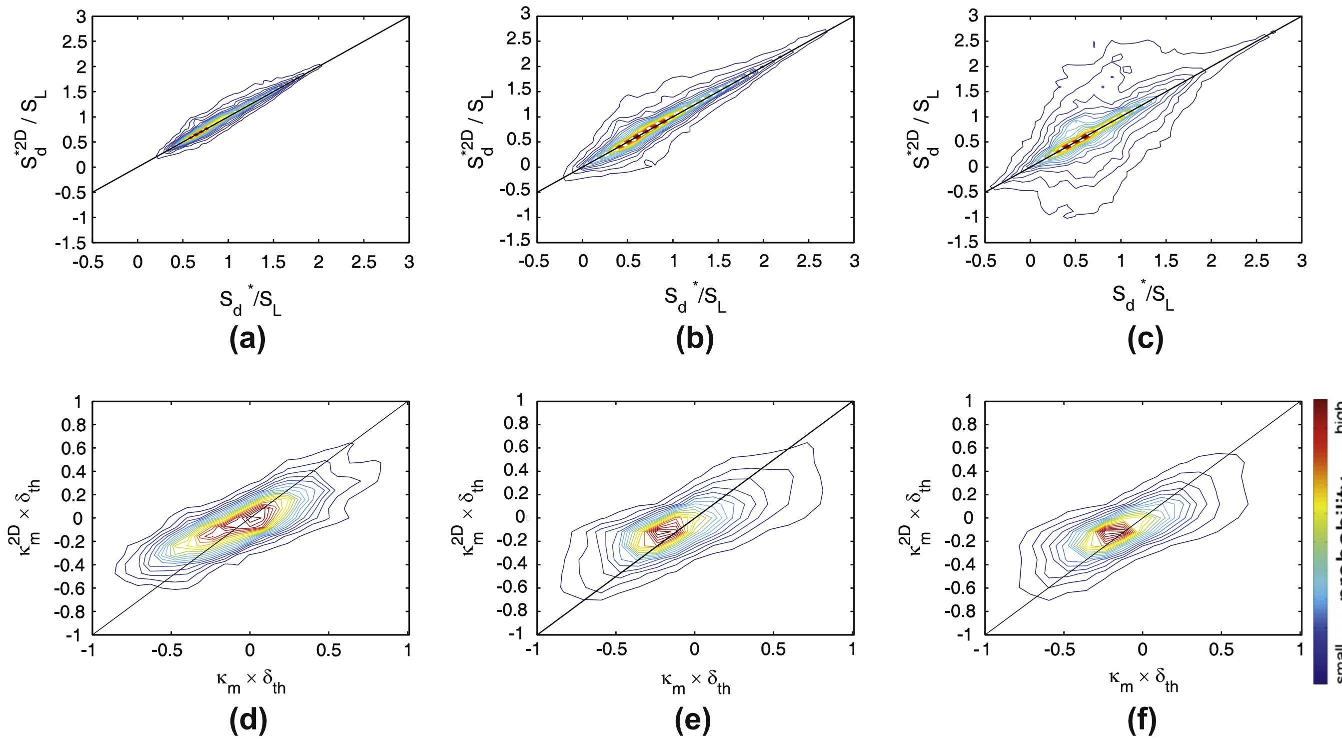

Fig. 10. Contours of joint pdf between S_d^{*2D}/S_L and S_d^*/S_L for: (a) case A, (b) case C and (c) case E on the $c = 0.8$ isosurface. Contours of joint pdfs between κ_m^{2D} and κ_m on the $c = 0.8$ isosurface for: (d) case A, (e) case C and (f) case E on the $c = 0.8$ isosurface. The black line with slope equal to unity in Fig. 10a–f corresponds to the line indicating a correlation coefficient equal to unity.

density-weighted displacement speed S_d^{*2D} based on time-resolved planar imaging. This warrants a direct comparison between S_d^{*2D} and the full three-dimensional density-weighted displacement speed S_d^*, which motivated the present study. Quantitative comparisons were carried out to explore the relation between S_d^* and S_d^{*2D} using a DNS database of statistically planar turbulent premixed flames. It has been found that the pdfs of S_d^{*2D} faithfully represent the pdfs of S_d^* (e.g. the mean value and standard-deviation of S_d^{*2D} remain almost the same as those for S_d^*) when u' remains either smaller than or almost equal to $6S_L$. However, the pdfs of S_d^{*2D} become significantly wider than the pdfs of S_d^* for higher values of u' (e.g. $u' \geqslant 9S_L$). Despite the deteriorating agreement between the pdfs of S_d^{*2D} and S_d^* with increasing u', the mean value of S_d^{*2D} remains almost the same as the actual mean value of S_d^* for all cases considered here, but the standard-deviation of S_d^{*2D} remains greater than that of S_d^*. This indicates that the pdf of S_d^{*2D} may faithfully replicate the pdf of actual three-dimensional density-weighted displacement speed S_d^* for small values of turbulent Reynolds number $\mathrm{Re}_t \sim (u'/S_L)^4/\ Ka^2$ (e.g. $\mathrm{Re}_t \sim 20$ cases considered in the present study) but the pdf of S_d^{*2D} may not be representative of actual pdf of density-weighted displacement speed S_d^* for large values of turbulent Reynolds number Re_t (e.g. $\mathrm{Re}_t \sim 100$ cases considered in the present study).

It has been found that the pdfs of κ_m^{2D} and S_t^{*2D} are found to be narrower than their actual three-dimensional counterparts (i.e. κ_m and S_t^* respectively). A simple correction is proposed, by which the correct pdfs, mean and standard-deviation of κ_m and S_t^* can be accurately approximated from the pdfs, mean and standard-deviation of $\pi/2 \times \kappa_m^{2D}$ and $\pi/2 \times S_t^{*2D}$ respectively. As S_d^{*2D} pdfs are wider than S_d^* pdfs and S_t^{*2D} pdfs are narrower than S_t^* pdfs, the pdfs of $(S_r^* + S_n^*)^{2D}/S_L = S_d^{*2D}/S_L - S_t^{*2D}/S_L = S_d^{*2D}/S_L + 2\rho D\kappa_m^{2D}/\rho_0 S_L$ are found to be wider than the pdfs of combined reaction and normal diffusion component of density-weighted displacement speed $(S_r^* + S_n^*)/S_L$. This gives rise to a standard-deviation of $(S_r^* + S_n^*)^{2D}/S_L$, which is about the twice of the standard-deviation of its actual three-dimensional counterpart $(S_r^* + S_n^*)/S_L$ for all the cases considered here. However, the mean values of $(S_r^* + S_n^*)^{2D}$ remain close to the mean values of $(S_r^* + S_n^*)$ for all cases considered here. It has been found that loss of perfect correlation between two and three-dimensional quantities leads to differences between $(S_r^* + S_n^*)^{2D} - \kappa_m^{2D}$ and $(S_r^* + S_n^*) - \kappa_m$, and between $S_d^{*2D} - \kappa_m^{2D}$ and $S_d^* - \kappa_m$ correlations. The correlation between density-weighted displacement speed S_d^* and curvature κ_m are strongly negatively correlated for all the cases whereas the correlation between S_d^{*2D} and κ_m^{2D} turns out to be much weaker than its three-dimensional counterpart. Similarly the correlation between $(S_r^* + S_n^*)^{2D}$ and κ_m^{2D} is found to be qualitatively different from the correlation between their three-dimensional counterparts (i.e. the correlation between $(S_r^* + S_n^*)$ and κ_m). Two clearly defined positive and negative correlating branches have been observed in the correlation between $(S_r^* + S_n^*)$ and κ_m but no such behaviour has been observed for the correlation between $(S_r^* + S_n^*)^{2D}$ and κ_m^{2D}. This suggests that the S_d^{*2D} statistics need to be used carefully to infer on actual statistical behaviour of S_d^*, as the standard-deviation and local curvature responses may differ, but the mean values can be estimated from two-dimensional measurements relatively accurately as long as the imaging plane contains the mean direction of flame propagation and the mean flow velocity in the out-of-plane direction remains negligible.

Acknowledgments

The authors gratefully acknowledge the financial support provided by the EPSRC, UK. N.C. acknowledges many useful discussions with Dr. E.R. Hawkes.

Appendix A. Flame speed statistics for five different *c* isosurfaces across the flame brush

Table A1
Table A2

Table A1
Relevant mean values and standard-deviations of flame speeds on five different c isosurfaces across the flame brush when statistics were extracted (i.e. $t_{sim} = \delta_{th}/S_L$).

c	Case	μ_{SD}	σ_{SD}	μ_{SD}^{2D}/μ_{SD}	$\sigma_{SD}^{2D}/\sigma_{SD}$	$\pi/2 \times \sigma_{ST}^{2D}/\sigma_{ST}$	μ_{SRN}	σ_{SRN}	μ_{SRN}^{2D}/μ_{SRN}	$\sigma_{SRN}^{2D}/\sigma_{SRN}$
0.1	A	0.97	0.73	1.16	1.26	1.14	0.98	0.34	1.17	2.35
	B	0.96	0.76	1.20	1.31	1.14	0.96	0.34	1.20	2.54
	C	1.08	1.00	1.15	1.55	1.26	1.10	0.55	1.13	2.61
	D	1.41	1.04	1.02	1.85	1.34	1.40	0.69	1.02	2.77
	E	1.20	1.21	1.11	1.62	1.32	1.23	0.79	1.09	2.42
0.3	A	0.97	0.52	1.12	1.24	1.13	0.97	0.11	1.13	4.97
	B	0.97	0.54	1.14	1.26	1.14	0.97	0.10	1.14	5.34
	C	0.98	0.79	1.18	1.49	1.31	0.99	0.40	1.18	2.74
	D	0.98	0.70	1.11	2.22	1.31	1.01	0.30	1.09	5.11
	E	1.01	0.91	1.12	1.81	1.21	1.01	0.42	1.13	3.77
0.5	A	0.99	0.47	1.09	1.19	1.14	0.98	0.11	1.09	3.95
	B	0.99	0.48	1.10	1.18	1.14	0.99	0.11	1.10	4.00
	C	0.95	0.66	1.16	1.46	1.28	0.96	0.24	1.15	3.67
	D	0.90	0.65	1.10	2.04	1.35	0.93	0.40	1.08	3.33
	E	0.97	0.79	1.10	1.79	1.23	0.97	0.38	1.11	3.65
0.7	A	1.00	0.43	1.07	1.15	1.14	1.00	0.16	1.07	2.40
	B	1.01	0.45	1.07	1.13	1.14	1.01	0.16	1.07	2.45
	C	0.95	0.62	1.12	1.37	1.30	0.97	0.34	1.11	2.32
	D	0.86	0.66	1.08	1.80	1.33	0.90	0.49	1.05	2.41
	E	0.96	0.77	1.07	1.67	1.26	0.98	0.48	1.07	2.58
0.9	A	1.01	0.39	1.06	1.13	1.13	1.01	0.23	1.06	1.53
	B	1.02	0.41	1.06	1.11	1.14	1.02	0.23	1.06	1.59
	C	0.96	0.61	1.10	1.28	1.28	0.98	0.43	1.09	1.71
	D	0.84	0.66	1.06	1.64	1.36	0.89	0.66	1.03	1.70
	E	0.96	0.81	1.06	1.50	1.34	1.00	0.69	0.97	1.74

Table A2
The relevant values of correlation-coefficients on five different c isosurfaces when statistics were extracted (i.e. $t_{sim} = \delta_{th}/S_L$).

c	Case	$S_d^* - \kappa_m$	$(S_r^* + S_n^*) - \kappa_m$	$S_d^{*2D} - \kappa_m^{2D}$	$(S_r^* + S_n^*)^{2D} - \kappa_m^{2D}$	$S_d^* - S_d^{*2D}$	$\kappa_m - \kappa_m^{2D}$
0.1	A	−0.88	−0.40	−0.48	−0.20	0.75	0.79
	B	−0.90	−0.38	−0.48	−0.18	0.75	0.78
	C	−0.79	−0.39	−0.30	−0.10	0.75	0.78
	D	−0.62	−0.39	−0.06	−0.01	0.75	0.78
	E	−0.70	−0.39	−0.14	−0.04	0.75	0.78
0.3	A	−0.97	−0.65	−0.56	−0.19	0.78	0.78
	B	−0.99	−0.65	−0.57	−0.15	0.78	0.78
	C	−0.83	−0.27	−0.30	−0.04	0.61	0.73
	D	−0.85	−0.42	−0.09	0.04	0.28	0.74
	E	−0.85	−0.41	−0.18	−0.01	0.38	0.73
0.5	A	−0.97	−0.26	−0.61	−0.14	0.84	0.78
	B	−0.98	−0.31	−0.61	−0.12	0.84	0.78
	C	−0.92	−0.33	−0.34	−0.04	0.63	0.72
	D	−0.75	−0.21	−0.09	0.07	0.37	0.75
	E	−0.85	−0.34	−0.19	0.00	0.43	0.73
0.7	A	−0.93	0.13	−0.61	−0.04	0.87	0.78
	B	−0.93	0.07	−0.61	−0.04	0.88	0.78
	C	−0.82	−0.07	−0.36	0.04	0.70	0.72
	D	−0.68	−0.04	−0.10	0.12	0.46	0.72
	E	−0.77	−0.17	−0.19	0.03	0.51	0.73
0.9	A	−0.84	0.44	−0.57	0.12	0.89	0.79
	B	−0.85	0.38	−0.56	0.11	0.90	0.77
	C	−0.73	0.22	−0.33	0.13	0.75	0.72
	D	−0.49	0.33	−0.09	0.25	0.54	0.78
	E	−0.56	0.13	−0.16	0.11	0.60	0.72

References

[1] N. Peters, Turbulent Combustion, Cambridge University Press, Cambridge, 2000.
[2] N. Chakraborty, R.S. Cant, Phys. Fluids 19 (2007) 105101.
[3] N. Chakraborty, R.S. Cant, Proc. Combust. Inst. 32 (2009) 1445–1453.
[4] B. Renou, A. Boukhalfa, D. Peuchberty, M. Trinité, Proc. Combust. Inst. 27 (1998) 841–847.
[5] G. Hartung, J. Hult, R. Balachandran, M.R. Mackley, C.F. Kaminski, J. Appl. Phys. B 96 (2009).
[6] C.F. Kaminski, J. Hult, M. Aldén, Appl. Phys. B 68 (1999) 757–760.1.
[7] C.F. Kaminski, X.S. Bai, J. Hult, A. Dreizler, S. Lindenmaier, L. Fuchs, Appl. Phys. B 71 (2000) 711–716.
[8] H. Malm, G. Sparr, J. Hult, C.F. Kaminski, J. Opt. Soc. Am. A 17 (2000) 2148–2156.1.
[9] C.F. Kaminski, J. Hult, M. Aldén, S. Lindenmaier, A. Dreizler, U. Maas, M. Baum, Proc. Combust. Inst. 28 (2000) 399–405.
[10] R. Abu-Gharbieh, G. Hamarneh, T. Gustavsson, C.F. Kaminski, Opt. Express 8 (2001) 278–287.
[11] J. Hult, M. Richter, J. Nygren, M. Aldén, A. Hultqvist, M. Christensen, B. Johansson, Appl. Opt. 41 (2002) 5002–5014.
[12] R. Abu-Gharbieh, G. Hamarneh, T. Gustavsson, C.F. Kaminski, J. Math. Imaging Vision 19 (2003) 199–218.

[13] T. Echekki, J.H. Chen, Combust. Flame 106 (1996) 184–202.
[14] I.R. Gran, T. Echekki, J.H. Chen, Proc. Combust. Instit. 26 (1996) 211–218.
[15] J.H. Chen, H.G. Im, Proc. Combust. Inst. 27 (1998) 819–826.
[16] N. Peters, P. Terhoeven, J.H. Chen, T. Echekki, Proc. Combust. Inst. 27 (1998) 833–839.
[17] T. Echekki, J.H. Chen, Combust. Flame 118 (1999) 303–311.
[18] H.G. Im, J.H. Chen, Proc. Combust. Inst. 28 (2000) 1833–1840.
[19] N. Chakraborty, S. Cant, Combust. Flame 137 (2004) 129–147.
[20] K.W. Jenkins, M. Klein, N. Chakraborty, R.S. Cant, Combust. Flame 145 (2006) 415–434.
[21] N. Chakraborty, M. Klein, R.S. Cant, Proc. Combust. Inst. 31 (2007) 1385–1392.
[22] H. Pitsch, L. Duchamp De Lageneste, Proc. Combust. Inst. 29 (2002) 2001–2008.
[23] N. Chakraborty, R.S. Cant, Phys. Fluids 17 (2005) 65108.
[24] E.R. Hawkes, J.H. Chen, Proc. Combust. Inst. 30 (2005) 647–655.
[25] N. Chakraborty, Phys. Fluids 19 (2007) 105109.
[26] N. Chakraborty, E.R. Hawkes, J.H. Chen, R.S. Cant, Combust. Flame 154 (2008) 259–280.
[27] N. Chakraborty, M. Klein, Phys. Fluids 20 (2008) 065102.
[28] N. Chakraborty, M. Klein, Proc. Combust. Inst. 32 (2009) 1435–1443.
[29] I. Han, K.H. Huh, Proc. Combust. Inst. 32 (2009) 1419–1425.
[30] W. Kollmann, J.H. Chen, Proc. Combust. Inst. 27 (1998) 927–934.
[31] S.B. Pope, Int. J. Eng. Sci. 26 (5) (1988) 445–469.
[32] S.M. Candel, T. J Poinsot, Combust. Sci. Technol. 70 (1990) 1–15.
[33] R.S. Cant, S.B. Pope, K.N.C. Bray, Proc. Combust. Inst. 23 (1998) 809–815.
[34] M. Boger, D. Veynante, H. Boughanem, A. Trouvé, Proc. Combust. Inst. 27 (1998) 917–925.
[35] A. Trouvé, T.J. Poinsot, J. Fluid Mech. 278 (1994) 1–31.
[36] E.R. Hawkes, R. Sankaran, J. H. Chen, Proc. Combust. Inst. 33, doi:10.1016/j.proci.2010.06.019.
[37] A.A. Wray, Minimal Storage Time Advancement Schemes for Spectral Methods, NASA Ames Research Center, California, Report No. MS 202 A-1, 1990.
[38] R.S.Rogallo, Numerical Experiments in Homogeneous Turbulence, NASA Technical Memorandum 91416, NASA Ames Research Center, California, 1981.
[39] G.K. Batchelor, A.A. Townsend, Proc. Roy. Soc. A 194 (1948) 527–543.
[40] T. Poinsot, S.K. Lele, J. Comp. Phys. 101 (1992) 104–129.
[41] F. Charlette, D. Veynante, C. Meneveau, Combust. Flame 131 (2002) 159–180.
[42] E.R. Hawkes, J.H. Chen, Combust. Flame 138 (2004) 242–258.
[43] E.R. Hawkes, J.H. Chen, Proc. Combust. Inst. 30 (2005) 647–655.
[44] E.R. Hawkes, J.H. Chen, Combust. Flame 144 (2006) 112–125.
[45] R.W. Grout, Phys. Fluids 19 (2007) 105107.
[46] I. Han, K.Y. Huh, Combust. Flame 152 (2008) 194–205.
[47] S. Lee, S.K. Lele, P. Moin, Phys. Fluids A 4 (8) (1992) 1521–1530.
[48] C.J. Rutland, A. Trouvé, Combust. Flame 94 (1993) 41–57.
[49] N. Chakraborty, R.S. Cant, Numer. Heat Trans. A 50 (7) (2006) 623–643.
[50] S. Gashi, J. Hult, K.W. Jenkins, N. Chakraborty, R.S. Cant, C.F. Kaminski, Proc. Combust. Inst. 30 (2005) 809–817.
[51] J. Hult, S. Gashi, N. Chakraborty, M. Klein, K.W. Jenkins, S. Cant, C.F. Kaminski, Proc. Combust. Inst. 31 (2007) 1319–1326.
[52] G. Hartung, J. Hult, C.F. Kaminski, J.W. Rogerson, N. Swaminathan, Phys. Fluids 20 (2008) 035110.
[53] J. Hult, U. Meier, W. Meier, A. Harvey, C.F. Kaminski, Proc. Combust. Inst. 30 (2005) 701–709.
[54] C.F. Kaminski, Phys. Chem. Chem. Phys. 219 (2005) 747–774.
[55] B. Ayoola, R. Balachandran, J.H. Frank, E. Mastorakos, C.F. Kaminski, Combust. Flame 144 (2006) 1–16.
[56] R.S.M. Chrystie, I.S. Burns, J. Hult, C.F. Kaminski, Meas. Sci. Technol. 19 (2008) 125503.
[57] B. Ayoola, G. Hartung, C.A. Armitage, J. Hult, R.S. Cant, C.F. Kaminski, Exp. Fluids 46 (2009) 27–41.
[58] C. Heeger, B. Böhm, S.F. Ahmed, R. Gordon, I. Boxx, W. Meier, A. Dreizler, E. Mastorakos, Proc. Combust. Inst. 32 (2009) 2957–2964.
[59] D.C. Bingham, F.C. Gouldin, D.A. Knaus, Proc. Combust. Inst. 27 (1998) 77–84.
[60] D.A. Knaus, F.C. Gouldin, P.C. Hinze, P.C. Miles, SAE Trans. 108, Paper No. 1999-01-3543,1999.